

AUS Repository

Molecular Dynamics Simulation of Thermal Conductivity Enhancement of Copper-Water Nanofluid

Item Type	Thesis
Authors	Abou-Tayoun, Nayef Hussein
Download date	2026-03-16 05:33:51
Link to Item	http://hdl.handle.net/11073/2765

MOLECULAR DYNAMICS SIMULATION OF THERMAL CONDUCTIVITY
ENHANCEMENT OF COPPER-WATER NANOFUID

A THESIS IN CHEMICAL ENGINEERING

Presented to the faculty of the American University of Sharjah
College of Engineering
in partial fulfillment of
the requirements for the degree

MASTER OF SCIENCE

By
NAYEF HUSSEIN ABOU-TAYOUN
B.S. American University of Sharjah
(2006)

Sharjah, U.A.E
Jan. 2012

© 2012

NAYEF HUSSEIN ABOU-TAYOUN

ALL RIGHTS RESERVED

We approve the thesis of Nayef Abou-Tayoun

Date of signature

Dr. Rachid Chebbi
Professor
Department of Chemical Engineering
Thesis Advisor

Dr. Naif Darwish
Professor
Department of Chemical Engineering
Graduate Committee

Dr. Oussama El-Kadri
Assistant Professor
Department of Chemistry
Graduate Committee

Dr. Zarook Shareefdeen
Associate Professor
Department of Chemical Engineering
Graduate Committee

Dr. Dana M. Abouelnasr
Department Head
Department of Chemical Engineering

Dr. Hany El-Kadi
Associate Dean, College of Engineering

Dr. Yousef Al-Assaf
Dean, College of Engineering

Dr. Khaled Assaleh
Director, Graduate Studies

MOLECULAR DYNAMICS SIMULATION OF THERMAL CONDUCTIVITY
ENHANCEMENT OF COPPER-WATER NANOFLUID.

Nayef Hussein Abou-Tayoun, Candidate for the Master of Science in Chemical
Engineering

American University of Sharjah, 2011

ABSTRACT

Nanofluid contains suspended nanoparticles, base fluid and some additives can be used for fluid stability like oleic acid and laurate salt. They are promising mediums to heat and cool high flux systems. Also, their use can extend to some other applications like photo-thermal therapy. That is why knowing the thermo-physical properties and especially the transport properties of the nanofluids are important to understand and implement their usage for many industrial applications and scientific studies. Molecular dynamics simulation (MD) is one of the tools that can be used to calculate these properties. In this work, the thermal conductivity of copper-water nanofluid was studied and calculated. The thermal conductivity of the nanofluid was found at different nanoparticles loading percentage ranging between 2.0-9.1% volume. The thermal conductivity of water was calculated and compared with the thermal conductivity value found in previous molecular dynamics works. The thermal conductivity of water found to be $0.77 \pm 0.01 \text{ W/m} \cdot \text{K}$ at 300 K and it was firstly calculated in order to obtain the enhancement ratio of the nanofluid at different volume percentages. The obtained data for thermal conductivity of copper-water nanofluid from the molecular dynamic simulation showed agreement with some experimental data. The highest obtained value of the thermal conductivity of

nanofluid was up to 84% at 300 K for 9.1% copper nanoparticle loading in water. Finally, the role of interatomic interaction in enhancing the thermal conductivity was observed.

Table of Contents

1. Introduction	1
1.1 Problem statement.....	1
1.2 Research significance	2
2. Literature review	3
2.1 What are nanofluids?	3
2.2 Nanofluids research concerns	5
2.3 Molecular simulations.....	9
2.4 Thermal conductivity models	11
3. Molecular dynamics theory and approach.....	14
3.1 Newtonian and Hamiltonian mechanics	14
3.2 Temperature	16
3.3 Pressure.....	17
3.4 Interatomic forces (potential forces).....	18
3.4.1. Water-water interatomic forces	18
3.4.2. Water-copper interatomic forces	21
3.4.3. Copper-copper interatomic forces	21
3.5 Intramolecular forces	22
4. Simulation and analysis	23
4.1 Molecular dynamic software	23
4.2 Periodic boundary conditions (PBC).....	24
4.3 Starting up the simulation	25
4.3.1. Initial configuration	25
4.3.2. Initial velocity	26
4.4 Running the simulation.....	26
4.5 Analyzing the output.....	27
5. Results and discussions	30
5.1 Thermal conductivity of water.....	30
5.2 Thermal conductivity of nanofluid	36

5.2.1. Nanoparticle loading at $\varphi = 2.0\%$	38
5.2.2. Nanoparticle loading at $\varphi = 2.8\%$	42
5.2.3. Nanoparticle loading at $\varphi = 5.2\%$	46
5.2.4. Nanoparticle loading at $\varphi = 6.0\%$	50
5.2.5. Nanoparticle loading at $\varphi = 9.1\%$	54
5.3 Experimental data with MD results	58
5.4 Role of interatomic potential	60
6. Conclusion and recommendations	62
References	64

List of Figures

Figure 1: Different molecular simulation methods	2
Figure 2: Thermal conductivity of different materials [3].....	4
Figure 3: Annual SCI publications on nanofluids [14]	5
Figure 4: Thermal conductivity against volume fraction of nanoparticle at different packing clusters [21].	7
Figure 5: Choi and Yu schematic model of nanofluid [23].	8
Figure 6: Maxwell model (—), geometrical mean model (—) and Xuan-Li experimental data (■).	12
Figure 7: Velocity-Verlet algorithm	16
Figure 8: Lennard Jones pair's potential and pair's force.	19
Figure 9: Water molecule model	19
Figure 10: MS-DOS screen snapshot during running simulation	24
Figure 11: The interaction between the primary cell and the Imaginary cells.	25
Figure 12: Thermal conductivity of nanocolloid system [57]: λ "■", λ_{kk} "□", λ_{pp} "●", $\lambda_{CC+PC+CP}$ "●" and λ_{MX} "▼"	29
Figure 13: VMD snapshot of initial positions of 991 water monomers.	31
Figure 14: Temperature trend during the simulation.....	32
Figure 15: Density of water at 300 K.	33
Figure 16: Decay of heat autocorrelation function for water.	34
Figure 17: Thermal conductivity of water: a) focused scale, b) full scale, c) overall k. blue line for k, red line for k_{zz} , green line for k_{yy} and purple line for k_{xx}	35
Figure 18: VMD snapshot of initial positions of 991 water monomers and copper nanoparticle.	37
Figure 19: VMD snapshots of 2 vol% nanofluid: a) y-x direction (z-axis is out), b) y-z direction (x-axis is out), c) y-x direction (z-axis is in).	38
Figure 20: Temperature trend during the simulation.....	39
Figure 21: Decay of heat autocorrelation function of nanofluid.	40
Figure 22: Thermal conductivity of nanofluids against time evolution $\phi = 2.0\%$: a) focused scale, b) full scale, c) overall k. blue line for k, red line for k_{zz} , green line for k_{yy} and purple line for k_{xx}	41

Figure 23: VMD snapshots of 2.8 vol% nanofluid: a) y-x direction (z-axis is out), b) y-z direction (x-axis is in), c) y-x direction (z-axis is in).	42
Figure 24: Temperature trend during the simulation.....	43
Figure 25: Decay of heat autocorrelation function of nanofluid.	44
Figure 26: Thermal conductivity of nanofluids against time evolution $\phi = 2.8\%$: a) focused scale, b) full scale, c) overall k. blue line for k, red line for k_{zz} , green line for k_{yy} and purple line for k_{xx}	45
Figure 27: VMD snapshots of 5.2 vol% nanofluid: a) y-x direction (z-axis is out), b) y-z direction (x-axis is out), c) y-x direction (z-axis is in).	46
Figure 28: Temperature trend during the simulation.....	47
Figure 29: Decay of heat autocorrelation function of nanofluid.	48
Figure 30: Thermal conductivity of nanofluids against time evolution $\phi = 5.2\%$: a) focused scale, b) full scale, c) overall k. blue line for k, red line for k_{zz} , green line for k_{yy} and purple line for k_{xx}	49
Figure 31: VMD snapshots of 9.1 vol% nanofluid: a) y-x direction (z-axis is out), b) y-z direction (x-axis is in), c) y-x direction (z-axis is in).	50
Figure 32: Temperature trend during the simulation.....	51
Figure 33: Decay of heat autocorrelation function of nanofluid.	52
Figure 34: Thermal conductivity of nanofluids against time evolution $\phi = 6.0\%$: a) focused Scale, b) full scale, c) overall k. blue line for k, red line for k_{zz} , green line for k_{yy} and purple line for k_{xx}	53
Figure 35: VMD snapshots of 9.1 vol% nanofluid: a) y-x direction, b) y-z direction, c) y-x direction (z-axis is in).	54
Figure 36: Temperature trend during the simulation.....	55
Figure 37: Decay of heat autocorrelation function of nanofluid.	56
Figure 38: Thermal conductivity of nanofluids against time evolution $\phi = 9.1\%$: a) focused sale, b) full scale, c) overall k. blue line for k, red line for k_{zz} , green line for k_{yy} and purple line for k_{xx}	57

Figure 39: Thermal conductivity enhancement ratio of copper-water nanofluid. the present MD work "■", Xuan et al [61] with r=10nm " ▲", Xuan et al [62] with r=50nm "×", Xuan and Li (2000) " ◆", Xuan and Li (2003) "+", Zhu et al [63] and Sanker et al. MD result "●" 59

Figure 40: The present MD study showing: kinetic energy " ▲", Van- der Waals " ◆", Coulombic potentials "■" 61

ACKNOWLEDGMENTS

I would like first to thank Allah for giving me the support and the strength to produce this work.

I would also like to thank my advisor Dr. Rachid Chebbi, for his support, continuous help, and understanding and for giving me the freedom to perform the research that I like and guide me throughout my thesis.

I would like to thank my graduate committee members for reviewing the thesis.

Last but not least, I would like deeply to thank my parents, wife, brothers, and sisters for their love, encouragement, and unconditional support.

Introduction

"Molecular simulation is a bridge between experiment and theory"

Allen & Tildesley

1.1 Problem statement

The scope of this work is to find the thermal conductivity of copper-water nanofluid and compare the result with the available experimental data. It also draws attention to a proposed mechanism which leads to enhancement in thermal conductivity of nanofluids; this mechanism appears due to the increase in the interatomic interactions that arise from interatomic potentials between nanoparticles and base fluid particles. During literature review, it is found that Sanker [1] et al. performed molecular dynamics simulation to find the thermal conductivity of platinum-water nanofluid. That nanofluid model was rigorous, in terms of using interatomic and intramolecular interactions among the constituents in the nanofluid. The rigorous models can be employed for studying and explaining the enhancement mechanism of thermal conductivity in nanofluids. On the other hand, Sarker and Selvam [2] simulated the copper-argon as copper-water nanofluid; the model wasn't rigorous as Sanker et al. nanofluid model but it showed that the heavy mass of copper slows the Brownian movement of nanoparticles through the argon atoms. Furthermore, they concluded that the enhancement in the thermal conductivity of nanofluids can be related to a mechanism that was described as "localized convection field in fluids" and it is one of six proposed mechanisms that explain the enhancement in the thermal conductivity of nanofluids [2, 3, 4]. Finally, both groups applied the equilibrium molecular dynamics (EMD) using Green-Kubo relations in evaluating the Navier-Stokes transport coefficients. Experimental work was conducted on copper-water nanofluid at different volume percentage ranges which has used as comparison data for the result of the molecular dynamic simulation [5].

1.2 Research significance

The high development in computing power has enhanced the use of numerical computations and simulation tools in understanding complex systems. There is no doubt that molecular dynamic simulation is one of these tools that shows a great effectiveness in many disciplines like nanotechnology, biophysics and catalysis. In general, molecular simulation is a bridge between experiment and theory [6]; therefore, molecular simulation can test theoretical models and compare the results with the data obtained from experiments. The molecular simulation works on nanoscopic scale instead of macroscopic scale, hence it gives us the chance to skip the process of setting up the experiment apparatus, bulk sampling and repeating trials; instead it gives us the ability to focus on understanding the phenomena by applying classical physics that is used in molecular dynamics, stochastic in Monte Carlo simulation or quantum physics in universal quantum simulator [7], Figure 1.

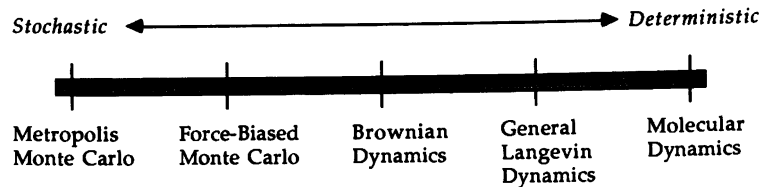


Figure 1: Different molecular simulation methods.

Furthermore, certain experiments are hard, expensive or not feasible to be carried out, so molecular simulation can be an affordable alternative to find the results of such experiments.

Sanker et al. [1], Sarker and Selvam [2] groups preformed molecular dynamics simulation to calculate the thermal conductivity of nanofluid. As in the problem statement, Sanker et al. group used the platinum-water nanofluid and compared it with copper-water nanofluid. Furthermore, Sarker and Selvam used copper-argon nanofluid instead of copper-water nanofluid. In the present work, the copper-water nanofluid was modeled; the extended simple point charge (SPC/E) model was used to represent the water monomers and Hamaker's potential function was used to mimic water-copper and copper-copper nanoparticles interactions. Moreover, the role of the interatomic interactions of nanofluid constituents in enhancing the thermal conductivity was studied.

Literature review

2.1 What are nanofluids?

In 1847, Michael Faraday reported that optical properties of gold colloids are different from those of corresponding bulk metal. This observation was considered as "the born of nanoscience" [8].

After Faraday observation, Maxwell presented conductivity effectiveness of heterogeneous solid suspensions [9]. Although particle-in-liquid suspensions or slurries have high thermal conductivity, they are not used in industries as heat transfer applications. Slurries have severe problems due to their suspended millimeter and micrometer particles' sizes. Such big particles settle rapidly and cause clogging, erosion, sedimentation and high pressure drop [10]. Moreover, water has the highest thermal conductivity (0.61W/mK at 300 K) among fluids that we use [11]; while metals like copper has one of the highest thermal conductivity (401 W/m K) among metals and metal oxides [12], as seen in Figure 2. So, it was found that adding metal nanoparticles in fluids like water or ethylene glycol can increase the thermal conductivity up to 40 % (Cu/EG) [13]. Such fluid -which has nano-sized particles less than 100 nanometer – has showed a promising usage in heat transfer and other applications.

The above described fluid is known to be *Nanofluid*. In general, nanofluid contains suspended nanoparticles, base fluid and some additives used for fluid stability like oleic acid and laurate salt [5]; the most used nanoparticles are metals, metal oxides, carbides and carbon nanotubes while the most used base fluids are water and ethylene glycol [10]. nanofluids are promising medium to heat and cool high flux systems like nuclear fission, fusion, micro/nanoelectronics and micro chemical reaction.

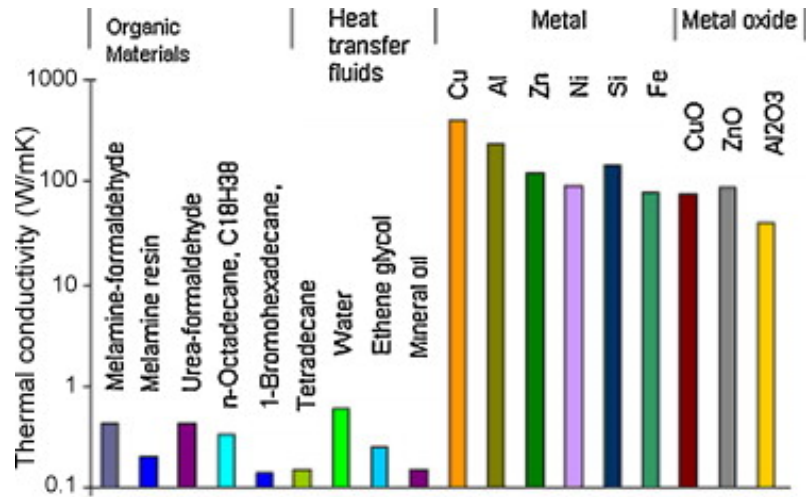


Figure 2: Thermal conductivity of different materials [3].

In general, it is believed that nanofluids gain its properties from the nanoparticles. Moreover, nanoparticles have high surface to volume ratio which makes them in nanofluids to be efficient to transfer energy and mass at high rates. The low mass of nanoparticles increases the colloidal stability of the nanofluid. Also, the low inertia of nanoparticles leads to low erosion velocity. A comparison between microparticles and nanoparticles is shown as in Table.1

Table 1: Comparison between microparticles and nanoparticles [10].

	Microparticles	Nanoparticles
Stability	Settle	Yes (Faraday's colloid 1857)
Erosion	High	No
Surface/volume ratio	Low	High (1000 time larger than Microparticles)
Conductivity	Low	High
Clogging	Yes	No
Pumping power	Large	Small

Furthermore, research in nanofluids has received attention worldwide; many prestigious universities such as M.I.T, Stanford University and the University of Leeds have established research centers and groups that concentrate on nanofluids [10]. In the past

few years, the publications in science citation index (SCI) journals have increased greatly as shown in Figure 3.

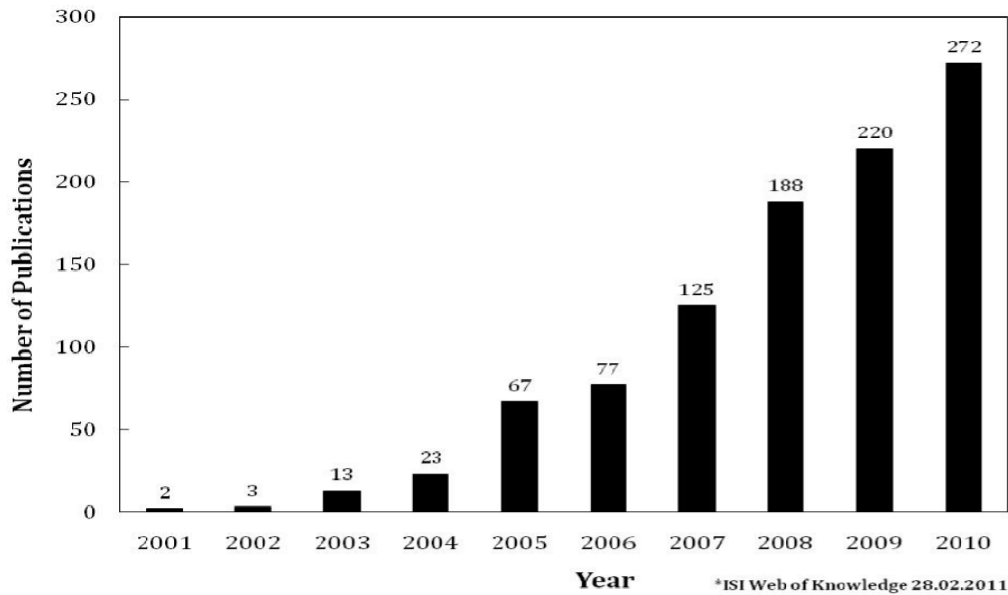


Figure 3: Annual SCI publications on nanofluids [14].

Figure 3 shows rapid growth of nanofluid researches and publications. It is estimated that the potential market for nanofluids will be over 2 billion dollars per year worldwide (CEA, 2007) [3].

2.2 Nanofluids research concerns

Studies have concentrated on many aspects of nanofluids; they have focused on nanofluids formulation, nanofluids applications, nanofluids physical-thermo properties and mechanistic understanding [3, 4].

Formulation of stable nanofluids is one of the most important issues. The nanofluid stability depends on many factors like the base liquid, particle concentration, particle size and the presence of a stabilizer. There are mainly two methods that can be used to formulate nanofluids, namely, the one-step method which is simply producing and dispersing the nanoparticles simultaneously in the nanofluid; this method is suitable in making nanofluids with stable metallic nanoparticles [15, 16]. Zhu et al. prepared copper-ethylene glycol nanofluid using the one-step method [15]. The two-step is another method where nanoparticles are made firstly and then dispersed in the nanofluid [5, 17]. Xuan and

Li prepared copper and copper oxide nanoparticles in water and oil transformer using the two-step method; they prepared the copper-water nanofluid to calculate the thermal conductivity.

Furthermore, nanofluids can be used in engineering and medical applications. In engineering, the trend of miniaturization in electronics and microelectromechanical systems (MEMS) have increased in the past 40 years [18]; on the same time such small systems generate lot of heat during operation and coolants with mirco-sized solid would affect the flow regime in the mirochannels and cause as what has been shown in Table .1. Thus, nanofluids as coolant mediums can be the solution for flowing smoothly in the microchannels.

As a biomedical application, magnetic nanoparticles in body fluids can be used as delivery vehicles for drugs or radiation providing new cancer treatment techniques [18]. El-Sayed et al. are one of the pioneers in using nanoparticles to heal tumors. They [19] mentioned in their paper that gold nanoparticles can first be used to absorb and scatter light strongly, a property that is used in sensing, imaging, and medical diagnostic then the absorbed light is rapidly converted into heat which is useful in photothermal therapy, like destroying cancer cells and surrounding them when their localized surface plasmon oscillations are excited.

Furthermore, a lot of research and experimental work on nanofluids focus on finding the physical-thermo properties like viscosity, critical heat flux (CHF) and thermal conductivity [3, 18]. These physical-thermo properties have important roles while studying and implementing nanofluid in improving the heat transfer efficiency and other different usages. Regime flow is one the most important aspect of nanofluid where viscosity is a main parameter. So, many experiments have been done on finding the viscosity of nanofluids. For instance, Putra et al. [20] measured the viscosity of Al_2O_3 -water and CuO-water nanofluids as function of shear rate and showed the Newtonian behavior of these nanofluids ranging between 1-4% [20]. Also, Das et al. [21] showed that the viscosity of Al_2O_3 -water nanofluid increases as the volume fraction of nanoparticles increase.

Lot of researches has been done in order to understand the mechanism of enchantment in the thermal conductivity of nanofluids. Koblinski and Eastman [21] proposed four

mechanisms explaining the enhancement of thermal conductivity of nanofluids: 1) Brownian motion of the particles, 2) molecular-level layering of liquid at the fluid-nanoparticle interface 3) the nature of heat transport in the nanoparticles, and 4) the effect of nanoparticle clustering. The first proposed mechanism analyzed and found that the Brownian diffusion of nanoparticle is 25-500 times slower than the thermal diffusion. Therefore, it concluded that the Brownian motion doesn't affect the thermal conductivity directly but possibly indirectly by producing nanoparticles clusters. Moreover, the molecular-level layer of liquid at the nanoparticle interface enhance the thermal conductivity; the atomic structure of liquid layers is more ordered than the bulk liquid and it leads to higher thermal conductivity. In primary, the heat is transported in metals though electrons and which also exhibits diffusion motion at macroscopic level. Koblinski and Eastman mentioned that the ballistic phonon between nanoparticles enhance the thermal conductivity of nanofluid. The fourth proposed mechanism showed the effect of the packing of nanoparticle clusters in enhancing the thermal conductivity of nanofluids, see below Figure 4.

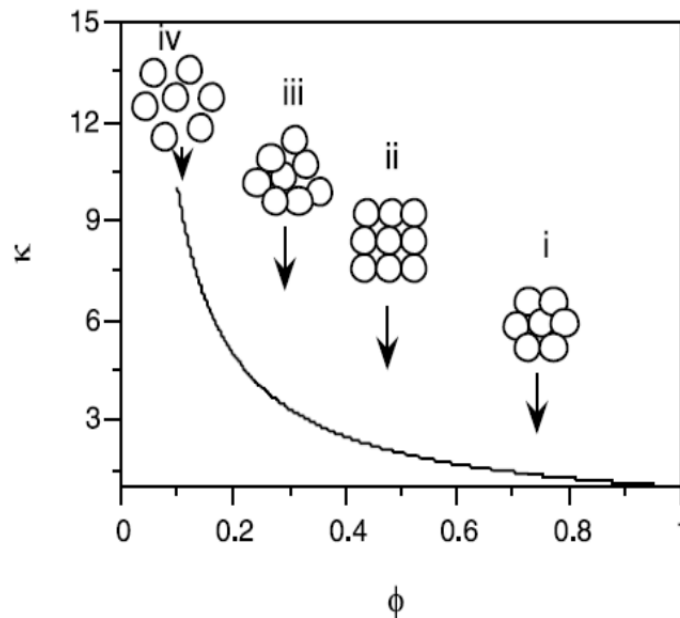


Figure 4: Thermal conductivity against volume fraction of nanoparticle at different packing clusters [21].

The figure shows that, the highly packed clusters of nanoparticles tend to have lower enhancement in thermal conductivity of nanofluid. On the other hand, clusters of nanoparticles separated by liquid layers are thin enough to allow for rapid heat flow among particles. Finally, Koblinski and Eastman suggested using modeling and molecular simulation in order to complement the experimental work and provide information that might be impossible to be obtained experimentally.

Also, Xuan and Li [5] mentioned other possible justifications for the enhancement of thermal conductivity of nanofluids: 1) The suspended nanoparticles increase the surface area and the heat capacity of the nanofluid 2) the suspended nanoparticles increase the effective (or apparent) thermal conductivity of the nanofluid 3) the interactions and collisions between nanoparticles and fluid particles are intensified 4) the mixing fluctuation and turbulence of the nanofluids are intensified 5) the dispersion of nanoparticles flattens the transverse temperature gradient of the fluid.

Some researchers used the concept of liquid-solid interfacial layer in order to explain the mechanism of heat transfer enhancement. Choi and Yu [23] suggested that the base fluid makes nanolayers around the nanoparticles (see Figure 5). The nanolayer can work as a bridge between the base fluid and the nanoparticles; therefore it enhances the thermal conductivity. It can be observed that Choi and Yu proposed mechanism was closer to the one that Koblinski and Eastman [12] mentioned

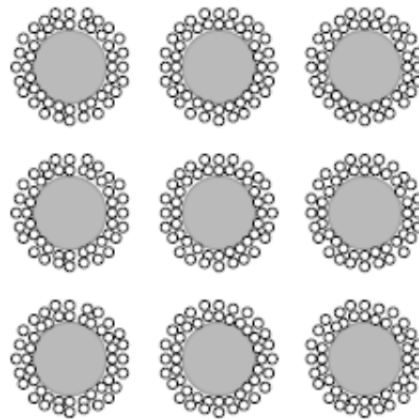


Figure 5: Choi and Yu schematic model of nanofluid [23].

Yet, there are much of controversies toward understanding the mechanism of the thermal conductivity enhancement in nanofluids. Lot of research works have been

conducted over this part; and it suggested different mechanisms and models but so far there is no absolute agreement on the mechanism.

2.3 Molecular simulations

The first use of molecular simulation was during the Manhattan project during Second World War; Enrico Fermi was a pioneer in using Monte Carlo (MC) method to study neutron transport in various types of nuclear systems [24]; the method was employed using FERIMAC which was invented by Fermi to assist in studying the neutron transport. After few years and by Wood and Parker, Monte Carlo method was carried out for soft-spheres where it introduced the Lennard-Jones interaction [25, 26]. The first use of molecular dynamic simulation was by Alder and Wainwright who simulated hard spheres using molecular dynamics; it was the first time to find dynamic properties without approximations [26, 27]. The implementation of Lennard-Jones, which represents kind of Van der Waal interactions in molecular dynamic simulation, had been firstly considered by Aneesur Rahman.

Rahman [28] was a pioneer in applying molecular dynamics for soft-spheres system. He used Lenard Jones potential function as an interaction potential between 864 Argon particles, using CDC 3600 computer machine. His algorithm was advanced and still in use in many codes of molecular dynamic simulation. In addition, Loup Verlet had calculated the phase diagram of argon liquid using the same molecular dynamics model of Rahman [28, 29]. The main achievements in Verlet's work are the bookkeeping device "Verlet neighbor list" which reduced the computation time of the order 10 and decreased computational errors [29]. Currently, this algorithm is used heavily in molecular dynamic simulation.

Molecular dynamics can be defined as one of the molecular simulation that computes the phase space trajectories of atoms or molecules. These phase space trajectories obey the classical Newtonian or Hamiltonian equations. In general, molecular dynamics is used in calculating the static and dynamic properties of the many-body systems. Moreover, molecular dynamics simulation has been used in equilibrium molecular dynamics (EMD) which has been able to predict the phase transition and phase equilibria. Also, the molecular dynamics simulation has the techniques to calculate the transport

coefficients using non-equilibrium molecular dynamic (NEMD). In addition, Green-Kubo relation is an exact mathematical expression that makes the use of equilibrium data produced from molecular simulation to predict the non-equilibrium properties using time correlation functions [30, 31, 32].

Furthermore, molecular dynamic simulation is used in finding transport coefficients for water as well as nanofluids. In literature, thermal conductivity and viscosity of water have been studied extensively [1, 2, 33, 34].

Several models have been used in modeling water monomers, including the simple point charge (SPC) (2-site model), the extended simple point charge (SPC/E) (3-site model extending the SPC model), and the n-point transferable intermolecular potential (TIPnP) model (n-site model with n ranging from 3 to 6) [33]. The extended simple point charge (SPC/E) model was proved in many molecular dynamic simulation works to be a good water monomer model [33, 35]. In fact, water is one of the most difficult fluids to model and study [25]. In the SPC/E model, monomers can be treated as rigid or flexible molecules [36, 37]. Flexible molecules model, which accounts for stretching atomic bonds and bending the angle between connected atoms, requires a quantum-mechanical treatment and a variable integration time step [36, 37]; therefore this complications were not considered in this work with the intramolecular potential discarded and instead rigid molecular model was used.

The thermal conductivity of water was found by reverse non-equilibrium molecular dynamic (RNEMD) [38] to be $\lambda=0.81 \pm 0.01 \text{ W/m} \cdot \text{K}$ at 300 K. Also, it was found by equilibrium molecular dynamics (EMD) via Green-Kubo [35] to be $0.67 \pm 0.04 \text{ W/m} \cdot \text{K}$ at 300 K. The experimental value of thermal conductivity of water [11] is $0.61 \text{ W/m} \cdot \text{K}$ at 300 K.

In addition, the thermal conductivity of nanofluid was done using EMD by Sanker et al. Sarker and Selvam. Experimentally, Xuan and Li [5] conducted nanofluid experiments to find the thermal conductivity of copper-water, copper-transformer oil, copper oxide-water and copper oxide-transformer oil. Sanker et al. performed MD to find the thermal conductivity of platinum-water nanofluid and compared it with copper-water experimental data. Also, Sarker and Selvam carried out MD to find the thermal conductivity of copper-water and it was compared with the experimental data [5].

2.4 Thermal conductivity models

The Maxwell's model [39] is one of the first classical models that are used to predict the electrical and thermal conductivity of micrometer and large-size particles of liquid-solid heterogeneous systems. For small volume fraction ϕ and spherical particles, the thermal conductivity enhancement of nanofluid using Maxwell's model is represented as follows

$$\frac{k_{nf}}{k_{bf}} = 1 + \frac{3\left(\frac{k_p}{k_{bf}} - 1\right)\phi}{\left(\frac{k_p}{k_{bf}} + 2\right) - \left(\frac{k_p}{k_{bf}} - 1\right)\phi} \quad (2.1)$$

Where k_p , k_{bf} and k_{nf} are thermal conductivity of nanoparticles, base fluid and nanofluid, respectively.

Hamilton-Crosser rewrites the Maxwell above model in order to cover nanofluid with non-spherical nanoparticles; it becomes as follows

$$\frac{k_{nf}}{k_{bf}} = 1 + \frac{\frac{k_p}{k_{bf}} + (n-1) - (n-1)\left(1 - \frac{k_p}{k_{bf}}\right)\phi}{\frac{k_p}{k_{bf}} + (n-1) + \left(1 - \frac{k_p}{k_{bf}}\right)\phi} \quad (2.2)$$

So, $n=3$ for spherical particles and $n=6$ for cylindrical particles.

Although other classical models are used to estimate the thermal conductivity of heterogeneous liquid-solid systems like Jeffery [40], Davis [41], and Bruggeman [42]; all such models underestimate the enhancement of thermal conductivity of nanofluids [43]. The thermal conductivity of nanofluids need models that consider the proposed mechanism like Brownian motion, interatomic interaction, nanolayer at liquid-solid interface. Choi and Yu are one of the pioneers in modifying the classical models of Maxwell and Hamilton-Crossers to count for their proposal mechanism of nanolayers [23], as seen in previous Figure 5.

Furthermore, many researchers have modified the Maxwell model in order to increase the accuracy of the thermal conductivity of nanofluids [18]. As mentioned previously, the thermal conductivity enhancement of nanofluids is possibly due to 6 proposed mechanisms:

- Brownian motion of nanoparticles in the base fluid that induce heat exchange.
- Brownian motion of nanoparticles creates a localized convection in fluid.
- High heat conduction for metallic nanoparticles.
- Nanoparticles clustering that increase the diameter.

- Nanolayers around nanoparticles play role in transferring heat to water molecules
- Thermal Enhancement transfer due to increased interatomic interactions arising from interatomic potential.

The above have been considered along with Maxwell's model so Koo-Kleinstreuer-Li (KKL) correlation [43] is obtained;

$$\frac{k_{nf}}{k_{bf}} = 1 + \frac{\frac{k_p}{k_{bf}} + (n-1) - (n-1)(1 - \frac{k_p}{k_{bf}})\varphi}{\frac{k_p}{k_{bf}} + (n-1) + (1 - \frac{k_p}{k_{bf}})\varphi} + 5 \times 10^4 \beta \varphi \rho_p c_p \sqrt{\frac{k_B T}{\rho_p D}} f(T, \varphi) \quad (2.3)$$

Where k_B is Boltzmann constant, T is the ambient temperature, ρ_p density of nanoparticles, c_p is the heat capacity of nanoparticles and D is the nanoparticles diameter. The empirical functions of β and $f(T, \varphi)$ capture the influences of particle diameter, temperature and volume fraction of nanoparticles. In general and as seen in equation (2.3), the first part represents the Maxwell model while the second part counts for the Brownian motion of the nanoparticles.

Warrer and Teja have modified a Geometrical Mean Model using Landau Lifshitz relation for thermal conductivity of heterogeneous materials [44].

$$(k_{nf})^n = (k_{nf})^n \varphi + (k_{bf})^n (1 - \varphi) \quad -1 < n < 1 \quad (2.4)$$

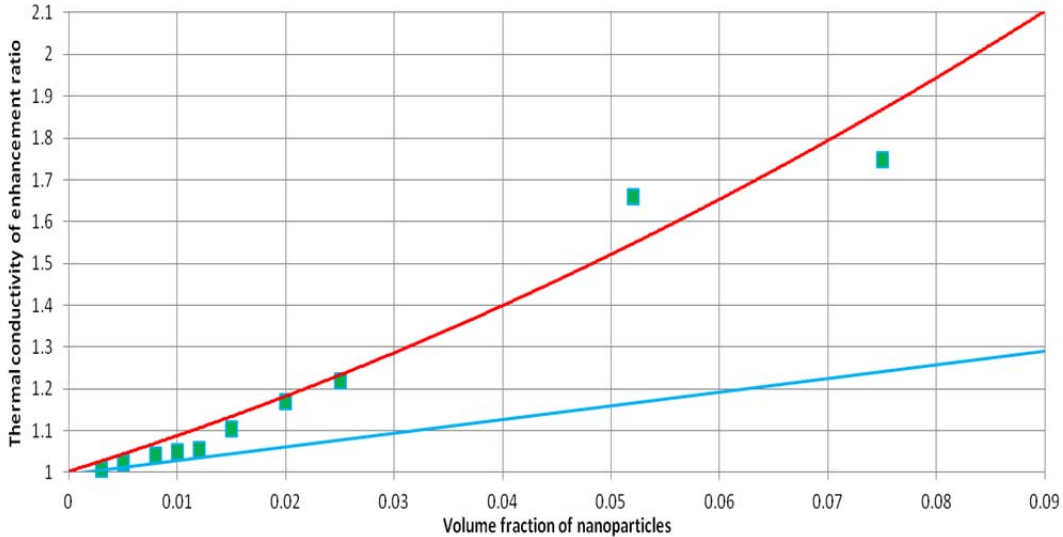


Figure 6: Maxwell model (—), geometrical mean model (—) and Xuan-Li experimental data (■).

For Xuan and Li copper-water experimental data, n is taken be 0.08. The Maxwell model, geometrical mean model and Xuan-Li experimental data are plotted as seen in Figure 6.

In general, the quest for a model that can predict the thermal conductivity of nanofluid is still ongoing. Computationally, molecular simulation may be the best tool to predict accurately the thermal conductivity and other transport coefficients of nanofluid.

Molecular dynamics theory and approach

"Make everything as simple as possible, but not simpler"

Albert Einstein

This chapter illustrates the modeling details and the computational methods that are used in performing the molecular dynamics simulation. It gives details of evaluating the temperature, pressure and the interatomic forces during the simulation. Moreover, Lennard-Jones is used to represent water-water interaction while Hamaker formula is used to represent copper-water and copper-copper interaction.

3.1 Newtonian and Hamiltonian mechanics

Many-body system of N atoms or molecules have $6N$ degrees of freedom or a hyperspace of $6N$ -dimensions that needs the components of position vectors $\mathbf{r}_i(t)$ and the components of momentum vectors $\mathbf{p}_i(t)$ for solving the phase space trajectory [46]. Thus, the $6N$ phase space contains two parts: $3N$ -dimensional configurational space and $3N$ -dimensional momentum space. The positions $\mathbf{r}_i(t)$ and momentums $\mathbf{p}_i(t)$ can be found by solving the Newton's equation of motion equation (3.1) with initial positions and momentums.

$$F_i = m_i a_i = m_i \frac{d^2 r_i}{dt^2} \quad (3.1)$$

Where r_i is the position of atom I , m_i is the mass of atom I and a_i is the acceleration of atom I .

The momentum p_i can be defined as:

$$p_i = m_i v_i \quad (3.2)$$

Where v_i is the velocity of atom i .

For the isolated system, the total energy (E), that has the kinetic and potential energy of the atoms or molecules, is conserved. The total Energy (E) can be identified as Hamiltonian. For N spherical molecules of atoms, the Hamiltonian equation has the following form

$$H(r, p) = \frac{1}{2m} \sum_i p_i^2 + U(r_1 + r_2 + \dots r_N) = E \quad (3.4)$$

Also, the forces on each molecule can be related to the potential function by

$$\frac{dU}{dr_i} = -\dot{p}_i = -m_i a_i = -F_i \quad (3.5)$$

In molecular dynamic simulation, Newton's equation of motion equation (3.1) can be solved using velocity-Verlet algorithm; this algorithm is one of the most used algorithms and it is simpler than basic Verlet algorithm. The basic Verlet is derived by writing the Taylor expansions of position in forward and backward in time.

$$r(t + \Delta t) = r(t) + v(t)\Delta t + \frac{1}{2} a(t)\Delta t^2 + \frac{1}{2} b(t)\Delta t^2 + O(\Delta t^4) \quad (3.6)$$

$$r(t - \Delta t) = r(t) - v(t)\Delta t + \frac{1}{2} a(t)\Delta t^2 - \frac{1}{2} b(t)\Delta t^2 + O(\Delta t^4)$$

(3.7)

Adding equation (3.6) and equation (3.7) gives:

$$r(t + \Delta t) = 2r(t) - r(t - \Delta t) + a(t)\Delta t^2 + O(\Delta t^4) \quad (3.8)$$

The positions $r(t)$ and $r(t - \Delta t)$ are both needed to solve Newton equations. Initially ($t = 0$), the prior position $r(t - \Delta t)$ is not known; therefore, the following equations are used to update the positions and velocities:

$$r(t + \Delta t) = r(t) + v(t)\Delta t + \frac{1}{2} a(t)\Delta t^2 + O(\Delta t^4) \quad (3.9)$$

$$v(t + \Delta t) = v(t) + \frac{a(t) + a(t + \Delta t)}{2} \Delta t + O(\Delta t^2) \quad (3.10)$$

As shown in equation (3.9) and equation (3.10), the truncation error of the position equation varies as Δt^4 and it varies for velocity as Δt^2 . The standard implementation of the Velocity-Verlet algorithm is as follows [6]:

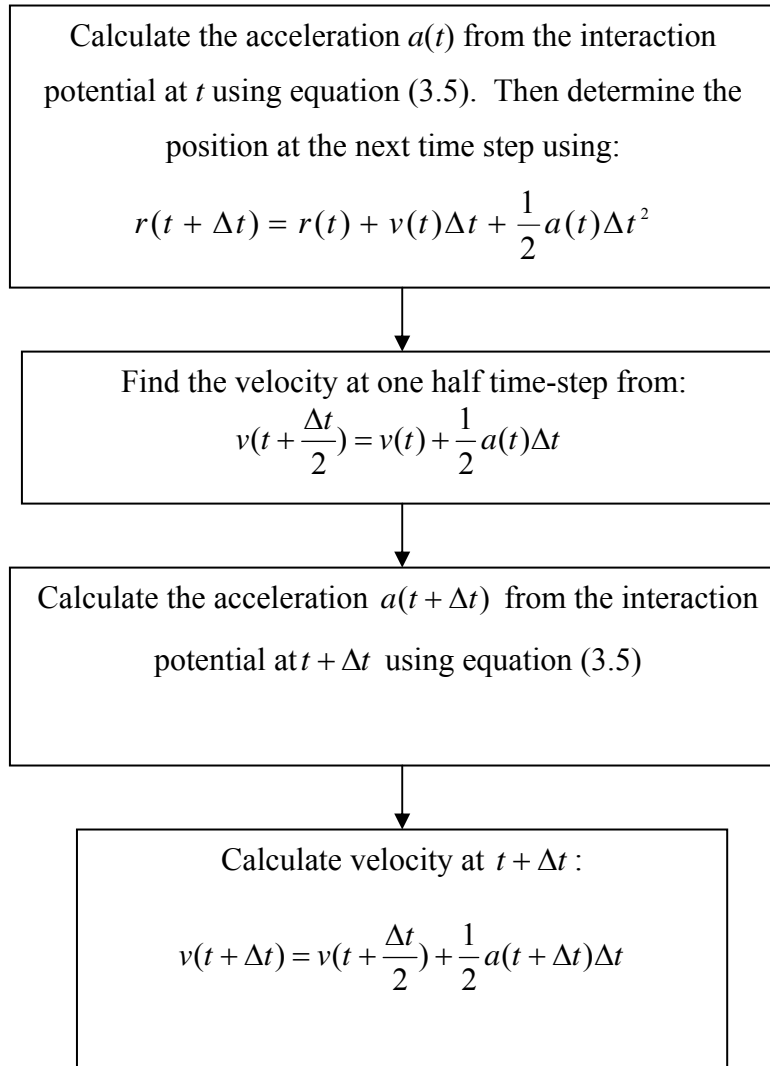


Figure 7: Velocity-Verlet algorithm.

3.2 Temperature

Simulation starts with initial configurations and velocities of atoms or molecules by assigning an average temperature. The average kinetic energy per degree of freedom is [45]:

$$\left\langle \frac{1}{2}mv^2 \right\rangle = \frac{1}{2}k_bT \quad (3.11)$$

Based on equilibration theorem, the kinetic energy of particle motion is equally distributed among all active degrees of freedom available for the particles. In this work, the flexible water monomer is a non-linear molecule that has 9 degree of freedom; it is distributed as 3 for translations, 3 for rotations and 3 for vibrations. The rigidity of water monomers in the bonds and angle eliminates the vibration and reduces the total number of degrees of freedom to $N_f = 6$. For single atom or pseudo single atom such as copper nanoparticle, the number of degrees of freedom is $N_f = 3$. The instantaneous temperature (3.12) fluctuates as the total kinetic energy does. It is given by:

$$T(t) = \sum_{i=1}^N \frac{m_i v_i^2(t)}{k_B N_{sf}} \quad (3.12)$$

where N_{sf} is the number of degrees of freedom of the system. The relative fluctuation in temperature is in the order of $1/\sqrt{N_{sf}}$ with N_{sf} typically in the order of 10^2 - 10^3 ; the statistical fluctuations in temperature are in order of 5-10%. To get an accurate estimate of temperature, one should average over many fluctuations [45].

3.3 Pressure

The pressure can be computed using the Virial equation of state [46] as

$$P = \rho kT - \frac{\rho}{3N} \left\langle \sum_{i<j} \sum r_{ij} \cdot \frac{dU(r_{ij})}{dr_{ij}} \right\rangle \quad (3.13)$$

The first term is the contribution of the ideal-gas and ρ is the number of molecules per volume; the second term is the contribution of the interatomic forces. The interatomic forces can be the most used potential functions like Lennard-Jones. For the soft spheres of liquids, the pressure exhibits larger fluctuations than the internal energy. Figure 8 shows that the large fluctuations are due to the highly changing of $r \frac{dU(r)}{dr}$ than does

$U(r)$ [46]:

$$\left| \frac{d}{dr} \left(r \frac{dU(r)}{dr} \right) \right| > \left| \frac{dU(r)}{dr} \right| \quad (3.14)$$

3.4 Interatomic forces (potential forces)

In this section, all the potential functions that were used to model the copper-water nanofluid were mentioned. Actually, there are three different interatomic forces that are applied in the copper-water nanofluid; these are water-water, water-copper and copper-copper.

3.4.1. Water-water interatomic forces

The interatomic potential $U(r^N)$ is assumed to be a pair additive; so the N atoms interaction energy is the sum of two-body contribution

$$U(r^N) = \sum_{i < j} u(r_{ij}) \quad (3.15)$$

The most important part for modeling a nano-sized system is to pick up the right potential functions to mimic the interactions among the nano-system constituents. In this work, copper-water nanofluid is the system that is modeled and simulated using molecular dynamics simulation.

In 1924, John Lennard Jones [47] proposed the first potential function for soft sphere of two bodies and it is known as Lennard potential function; it is expressed as

$$u(r) = 4\varepsilon \left(\left(\frac{\sigma}{r} \right)^{12} - \left(\frac{\sigma}{r} \right)^6 \right) \quad (3.16)$$

Where ε is the energy at minimum $u(r)$ and σ the distance at which the inter-particle potential is zero.

This is the simplest potential function and it is well-known to be a good approximation for noble gases; also it's suitable for many neutral atoms and molecules. Moreover, Lennard-Jones potential (LJ) function contains two terms; r^{-12} term represents the Paul repulsion at short distances due to the overlapping electron orbits and the r^{-6} term describes the Van der Waals attraction forces at long ranges. The force that is produced from the Lennard-Jones potential is

$$F(r) = -\frac{du(r)}{dr} = 24 \frac{\varepsilon}{\sigma} \left(2 \left(\frac{\sigma}{r} \right)^{13} - \left(\frac{\sigma}{r} \right)^7 \right) \quad (3.17)$$

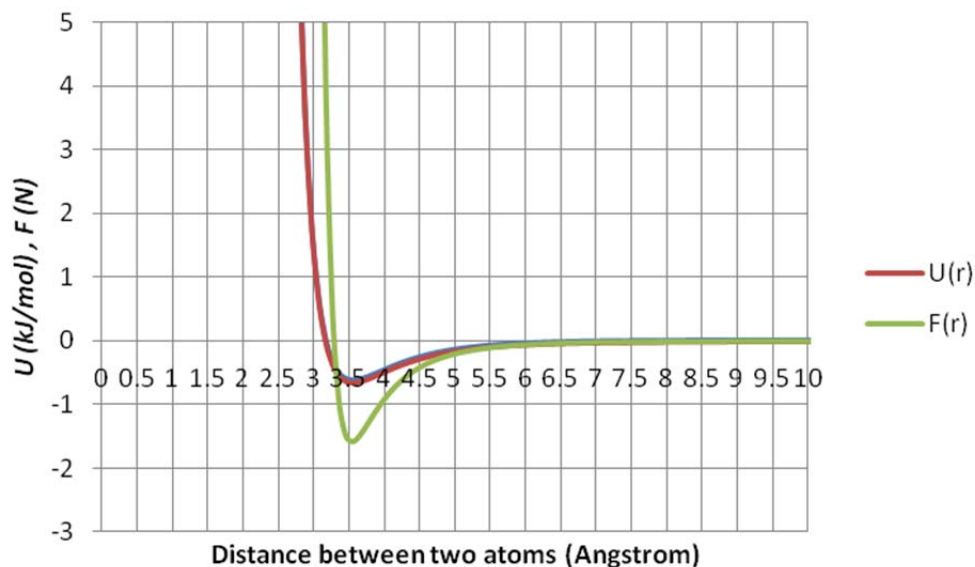


Figure 8: Lennard Jones pair's potential and pair's force.

Computing pair potential that extends over a wide range of pair separation is computationally costly; the common choice of truncation is at $r_c = 2.5\sigma$, at which $u = -0.0163\epsilon$ and $F = -0.039\epsilon/\sigma$ as seen in Figure 8.

For modeling the water-water interatomic potential, Lennard-Jones potential function with SPC/E (Simple Point Charge /Extended) [33] was used. The water (H_2O) has two Hydrogen atoms that are connected with an Oxygen atom through a covalent bond of 1.0 Å; the HOH angle is $\theta_o = 109.47^\circ$ [33].

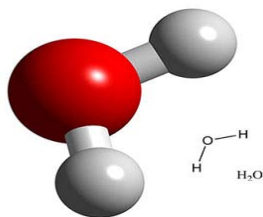


Figure 9: Water molecule model.

There are positive and negative charges on the two hydrogen atoms and oxygen atom, respectively. The coulomb term was added to the Lennard Jones potential in order to include the long-range interaction due to the charges contribution in the interatomic forces

[32]. Furthermore, Lennard Jones potential is used for O-O interaction as shown in the following equation (3.17) [6, 32],

$$u(r) = \underbrace{4\varepsilon_{oo} \left(\left(\frac{\sigma_{oo}}{r_{oo}} \right)^{12} - \left(\frac{\sigma_{oo}}{r_{oo}} \right)^6 \right)}_1 + \underbrace{k_e \sum_{a=1}^3 \sum_{b=1}^3 \frac{q_a q_b}{r_{ab}}}_2 \quad (3.17)$$

Where q_a is the charge on the atom a, q_b is the charge on atom b, k_e is coulomb constant ($k_e = 8.99 \times 10^9 \text{ N} \cdot \text{m}^2 / \text{C}^2$) and r_{ab} is the distance between two atoms. The Lennard Jones and the coulomb parameters are [33] $\sigma_{oo} = 3.5533 \text{ \AA}$, $\varepsilon_{oo} = 0.1553 \text{ kcal/mol}$, $q_o = -0.8476|e|$ and $q_H = 0.4238|e|$.

In equation (3.17), the Lennard Jones (1) is the first term decays faster as distance r increases while the Coulomb (2) is the second term that decays slower as r distance increases because it is a function of $1/r$. So, calculating the long-range interaction produces large errors and summation techniques are needed to avoid such errors.

Long-range interaction is one of the most expensive parts in computation; neglecting it gives the rise of serious inaccuracy. In order to solve this error, Ewald and particle-particle-mesh (PPPM) summations are one of the most used techniques in solving the long-rang interaction [45]. Although, Ewald is a preferable technique in molecular simulation, it scales as $O(N^{3/2})$. In the current work, the PPPM algorithm is used to overcome the Ewald expenses and calculate the electric potential term. The algorithm reduces computational time [48] in comparison with the Ewald summation method. PPPM scales as $O(N \log N)$ and it calculates the long-rang interaction in three steps [25]: 1) the electric charges are assigned to a finely-spaced mesh in the simulation box, 2) the fast Fourier transform is used to solve the Poisson equation for electrostatic potential due to the charge distribution on the mesh, 3) the potential at each mesh is calculated by numerically differentiation the potential and then the force on a particular particle i is calculated from the mesh field by interpolation. A value of 10^{-4} tolerance was selected while using the PPPM method.

3.4.2. Water-copper interatomic forces

Water-copper is the second type of the interatomic forces that exist in the nanofluid. Everaers and Ejtehadi [49] proposed, based on Hamaker's theory, the interaction function between colloid-colloid and solvent-colloid to be implemented in molecular simulations of mixtures; the colloid-solvent is used to describe the interatomic potential between the solvent and the colloidal particles (large particles).

$$U = \frac{2A_{cs}a^3\sigma^3}{9(a^2 - r^2)^3} \left[1 - \frac{(5a^6 + 45a^4r^2 + 63a^2r^4 + 15r^6)\sigma^6}{15(a-r)^6(a+r)^6} \right] \quad (3.16)$$

Where A_{cs} is the Hamaker's constant of water is taken to be $A_{cs} = 43.2 \text{ kcal/mol}$ [50, 51], "a" is the radius of the copper colloid. The sigma (σ) was taken as an arithmetic mixing between copper nanoparticle sigma and water sigma.

3.4.3. Copper-copper interatomic forces

Also, the Hamaker's formula for colloid-colloid was used to model the interaction potential between the copper nanoparticles

$$U_A = -\frac{A_{cc}}{6} \left[\frac{2a_1a_2}{r^2 - (a_1 + a_2)^2} + \frac{2a_1a_2}{r^2 - (a_1 - a_2)^2} + \ln \left(\frac{r^2 - (a_1 + a_2)^2}{r^2 - (a_1 - a_2)^2} \right) \right] \quad (3.17)$$

$$U_R = \frac{A_{cc}\sigma^6}{37800r} \left[\frac{r^2 - 7r(a_1 + a_2) + 6(a_1^2 + 7a_1a_2 + a_2^2)}{(r - a_1 - a_2)^7} + \frac{r^2 + 7r(a_1 + a_2) + 6(a_1^2 + 7a_1a_2 + a_2^2)}{(r + a_1 + a_2)^7} \right. \\ \left. - \frac{r^2 + 7r(a_1 - a_2) + 6(a_1^2 - 7a_1a_2 + a_2^2)}{(r + a_1 - a_2)^7} - \frac{r^2 - 7r(a_1 - a_2) + 6(a_1^2 - 7a_1a_2 + a_2^2)}{(r - a_1 + a_2)^7} \right] \quad (3.18)$$

$$U = U_A + U_R \quad (3.19)$$

where A_{cc} is the Hamaker's constant $A_{cc} = 107.83 \text{ kcal/mol}$ [52] and "a₁" and "a₂" are the radii of the pair of copper nanoparticles. The sigma (σ) is taken as an arithmetic mixing between the pair of copper nanoparticles.

3.5 Intramolecular forces

In polyatomic systems, the angles and bonds between the atoms give some flexibility of stretching and bending motions of the molecules. Although treating flexible molecules gives more accurate and precise result, classical molecular simulation shows serious errors in computing intramolecular forces of bonds and angles [36, 37]. In general, intramolecular bonds and angles are treated in quantum mechanics. Therefore, rigid molecules are used in this work to overcome the intramolecular computing complications. For water, the velocity-version of SHAKE algorithm has been used to make a rigid SPC/E model. Moreover, the copper nanoparticle is modeled as a Pseudo-single atom or all-atom which represents a group of copper atoms [37]. The velocity-version of SHAKE and the basic SHAKE have the same algorithms. Basic SHAKE is based on basic Verlet algorithm while the velocity-version of SHAKE is based on velocity-Verlet algorithm. There are many beneficial properties of the velocity-version of SHAKE over the basic SHAKE where the precision is one these main properties [53].

Simulation and analysis

"Everything that living things do can be understood in terms of the jiggling and wiggling of atoms"

Richard Feynman

This chapter introduces LAMMPS software which is used in this work to carry out the molecular dynamics simulations. The equilibrium molecular dynamics (EMD) via Green-Kubo is implemented to evaluate the thermal conductivity of copper-water nanofluid. Moreover, visual molecular dynamic (VMD) [54] software is used to get snapshots of the simulated samples of the nanofluids during time evolution.

3.6 Molecular dynamic software

Large-scale atomic/molecular massively parallel simulator (LAMMPS) [55] is general public license software (GNU) that was used to simulate the copper-water nanofluid system. LAMMPS has the ability to simulate soft materials (biomolecules, polymers), solid-state materials (metals, semiconductors) and coarse-grained or mesoscopic systems. Also, it can be used to model atoms or, more generally, as a parallel particle simulator at the atomic, meso, or continuum scale. Moreover, LAMMPS runs on single or on parallel processors using message-passing techniques and a spatial-decomposition of the simulation domain. The software contains the syntaxes and codes that are developed by many scholars and researchers. The codes and the algorithm are written in C++ and compiled by Cygwin.

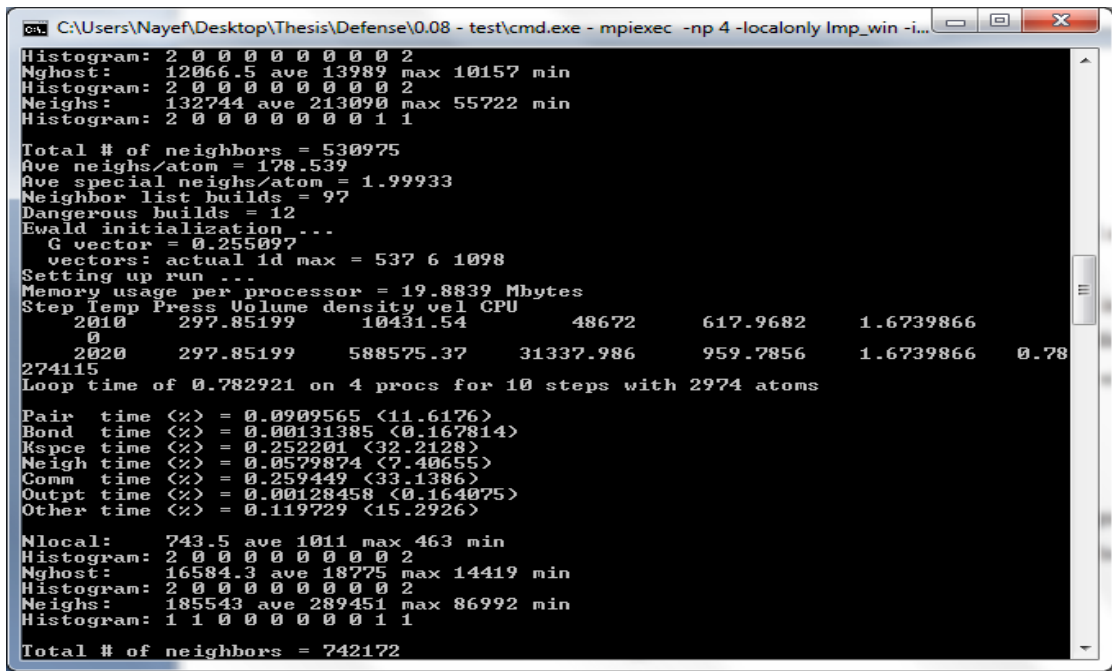
A) LAMMPS components:

1) LAMMPS input file:

The input file is a simulation box which contains elements that set the unit, boundary region, number of atoms and molecules, intra- and inter-molecular forces and thermodynamic ensembles (NPT, NVT and NVE). The detail of the input will be discussed later in this paper. The input file was executed in a MS-DOS.

2) LAMMPS output files:

LAMMPS generates two different outputs: the first output is a .XYZ file that contains the cartesian coordinates of each atom or molecule with respect to time evolution. The .XYZ file is converted to protein data bank (.PDB) which is useful in visualizing the atoms and molecules motion. Moreover, visualization molecular dynamics (VMD) is the software that was used to visualize the motion of the atoms and the molecules; it takes the .PDB file to show the nanofluid sample animation. The second output file contains the thermodynamic parameters and it was arranged as: step, temperature, pressure, volume, thermal conductivity coefficients and Van der Waals interaction; LAMMPS can show many other thermodynamic parameters. The thermodynamic parameters can be monitored as a display on MS-DOS screen and it was saved as a .log file. The log file can be used for further analysis of the data.



```

Histogram: 2 0 0 0 0 0 0 0 2
Nghost: 12066.5 ave 13989 max 10157 min
Histogram: 2 0 0 0 0 0 0 0 2
Neighs: 132744 ave 213090 max 55722 min
Histogram: 2 0 0 0 0 0 0 1 1

Total # of neighbors = 530975
Ave neighs/atom = 178.539
Ave special neighs/atom = 1.99933
Neighbor list builds = 97
Dangerous builds = 12
Ewald initialization ...
G vector = 0.255097
vectors: actual id max = 537 6 1098
Setting up run ...
Memory usage per processor = 19.8839 Mbytes
Step Temp Press Volume density vel CPU
2010 297.85199 10431.54 48672 617.9682 1.6739866
0 0 0 0 0 0
2020 297.85199 588575.37 31337.986 959.7856 1.6739866 0.78
274115
Loop time of 0.782921 on 4 procs for 10 steps with 2974 atoms

Pair time (%) = 0.0909565 (11.6176)
Bond time (%) = 0.00131385 (0.167814)
Kspce time (%) = 0.252201 (32.2128)
Neigh time (%) = 0.0579874 (7.40655)
Comm time (%) = 0.259449 (33.1386)
Outpt time (%) = 0.00128458 (0.164075)
Other time (%) = 0.119729 (15.2926)

Nlocal: 743.5 ave 1011 max 463 min
Histogram: 2 0 0 0 0 0 0 0 2
Nghost: 16584.3 ave 18775 max 14419 min
Histogram: 2 0 0 0 0 0 0 0 2
Neighs: 185543 ave 289451 max 86992 min
Histogram: 1 1 0 0 0 0 0 1 1

Total # of neighbors = 742172

```

Figure 10: MS-DOS screen snapshot during running simulation.

3.7 Periodic boundary conditions (PBC)

Molecular simulation is performed on finite number of molecules ranging from hundred to thousand. In order to mimic the infinite system, the simulated N molecules confined in

volume V should be bounded with free physical walls that are constructed by periodic boundary conditions. The volume V is the primary cell which is surrounded by its replicas called imaginary cells as seen in Figure 11.

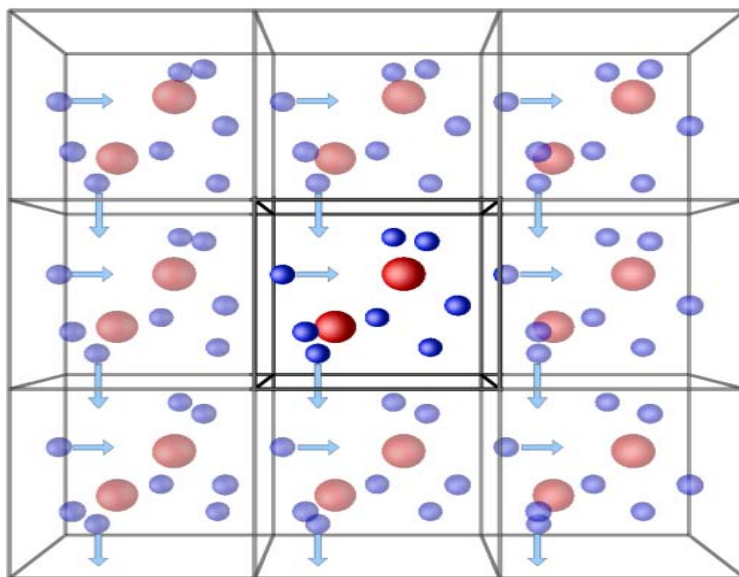


Figure 11: The interaction between the primary cell and the Imaginary cells.

The periodicity of the confined volume makes the primary cell interactive with the imaginary cells; so the molecule or atom that leaves through a particular bounding face will reenter the primary cell from the opposite face. Also, the atoms that are lying within distance r_c of boundary interact with the atoms of the opposite boundary.

3.8 Starting up the simulation

For solving the equation of motion, the initial molecular configuration and the initial velocity should be specified to each atom so the phase-space trajectories can be obtained during time evolution.

3.8.1. Initial configuration

The simplest way to construct the initial positions in the simulated region is to place the molecules randomly; but the molecular dynamic may face some difficulties in solving the stiff differential equations due to high intermolecular forces. Thus, each molecule was

assigned in the cubical simulation box while avoiding overlapping among the arranged atoms. The spacing between the N molecules in the confined volume identifies the density of the simulated system. During the simulation, new molecular arrangements appear and the initial configurations arrangement is forgotten.

In this simulation work, 991 water molecules were assigned in the lattice where the copper volume percentages were ranged between 2.0-9.1% of the nanofluid.

3.8.2. Initial velocity

Initial velocities of the molecules should be specified by choosing an initial temperature which was set at 300 K (room temperature). The initial velocities of the molecules were randomly chosen from Gaussian distribution. Like the initial configurations, the new molecular velocities appear where the initial set of the molecular velocities is forgotten after long time of running the simulation.

3.9 Running the simulation

After preparing the input file which was executed in LAMMPS, different output parameters like pressure, temperature, total energy, and density were displayed on MS-DOS. Tracking these outputs help in identifying the equilibration of the system. After some time, the temperature and the total energy should not show any change in their values in order to have an equilibrium system.

In addition, the canonical ensemble (NVT) has been used to set the simulated system and have constant number of molecules N , constant volume V and constant temperature T . In general, the system temperature can be set by using one of the thermostat techniques. The energy of the simulated system is conserved. Both the energy and temperature are related, so the temperature should be kept constant during the simulation. The use of the thermostat avoids temperature drifts because of the accumulation of numerical errors during molecular dynamics simulations [56].

The Nosé-Hoover thermostat algorithm has been used [57] for thermostating at 300 K while keeping the volume constant. The algorithm basically adds a friction term to Newton's equation, with the time rate of change of the friction coefficient, given as a

product of the relative deviation from the set value of temperature by the square of a relaxation rate

$$H_{Nose-Hoover} = \sum_{i=1}^N \frac{\bar{p}_i}{2m_i s^2} + U(r^N) + \frac{p^2 s}{2Q} + g k_b T \ln s \quad (4.1)$$

The expression provides a heat bath for thermostating and represents the extra degree of freedom. The first two terms represent the kinetic and potential energies of the system. The “g” term is the number of independent momentum degrees of freedom of the system which is 3N+1, N particles + 1 new degree of freedom. The “s” is the time scale parameter. The temperature “T” is the thermostat temperature. Furthermore, the “Q” is the magnitude of the coupling strength and should be set carefully. If Q is high, there will be a poor temperature control; and when Q is low, there will be an oscillating temperature.

3.10 Analyzing the output

Green-Kubo Formula is a mathematical expression that calculates transport coefficients like diffusion, viscosity and thermal conductivity. In this work, it was used to calculate the thermal conductivity of the copper-water nanofluid. The form of the formula is as follows [30, 31, 32]:

$$\lambda = \frac{1}{3k_B V T^2} \int_0^t \langle J(0)J(t) \rangle dt = \frac{\lambda_x + \lambda_y + \lambda_z}{3} \quad (4.2)$$

where λ is the thermal conductivity, V is the confined volume, T is the system temperature and J is the instantaneous microscopic heat current vector [2, 57]

$$J = \frac{d}{dt} \sum_{i=1}^N r_i \tilde{E}_i = \frac{d}{dt} \sum_{i=1}^N r_i (E_i - h) \quad (4.3)$$

Equation (4.3) is expressed as follows [58]

$$J = \sum_{k=\alpha}^{\beta} \sum_{i=1}^{N_k} \overbrace{\left(\frac{1}{2} m v_{ik}^2 (v_{ik})^2 v_{ik} \right)}^{K.E} + \sum_{k=\alpha}^{\beta} \sum_{l=\alpha}^{\beta} \sum_{i=1}^{N_k} \sum_{j>i}^{N_l} \left[\overbrace{IU(r_{ijkl})}^{P.E} + \overbrace{r_{ijkl} \frac{\partial U(r_{ijkl})}{\partial r_{ijkl}}}^C \right] \cdot v_{ik} - \sum_{k=\alpha}^{\beta} h_k \sum_{i=1}^{N_k} v_{ik} \quad (4.4)$$

The above expression of \mathbf{J} shows three modes; the first term represents the kinetic energy mode (K.E), the second term represents the potential energy mode (P.E), the third

term is the collision mode (C). The last term is the average enthalpy per atom h_v ; it is subtracted from the atomic energy and doesn't contribute to the heat flux [22]. \mathbf{I} is the unit tensor; " α ", " β " symbols denote the two different kinds of particles and " N " denotes the number of molecules or particles.

Although, the above expression of heat current vector is ideally for homogenous systems, it is used in the current work as other NEMD [2] and EMD [1, 59] studies done before; the heat flux expression shows a reasonable variation of 7.6% between NEMD and EMD [2]. Moreover, the average enthalpy per atom is excluded from heat current vector of this simulation due to its negligible effect in the thermal conductivity and it helps in reducing simulation complications [1, 59]. As it was mentioned before, the average enthalpy per atom is subtracted only from the K.E mode. In Figure 12, Eapen and Yip showed that the K.E mode is almost zero for nanocolloids systems so neglecting the K.E mode and the average enthalpy per atom is applicable [58]. As in equation (4.3), the heat current vector is a sum of three modes (K.E, P.E, and C); thus the conductivity can be expressed as a sum of nine terms which can be conveniently grouped together into self correlations, KK, PP, and CC and cross correlations PC, PK, etc [58]. In addition, CC+PC+CP contribute 90% of the overall value of the thermal conductivity and it is constant through a range of volume percentage of nanocolloid. The PP mode shows as the volume fraction increases a significant contribution in enhancing in thermal conductivity of the nanocolloid system. In the coming section, the effect of PP mode and the role of the interatomic potential in increasing the thermal conductivity was studied and discussed.

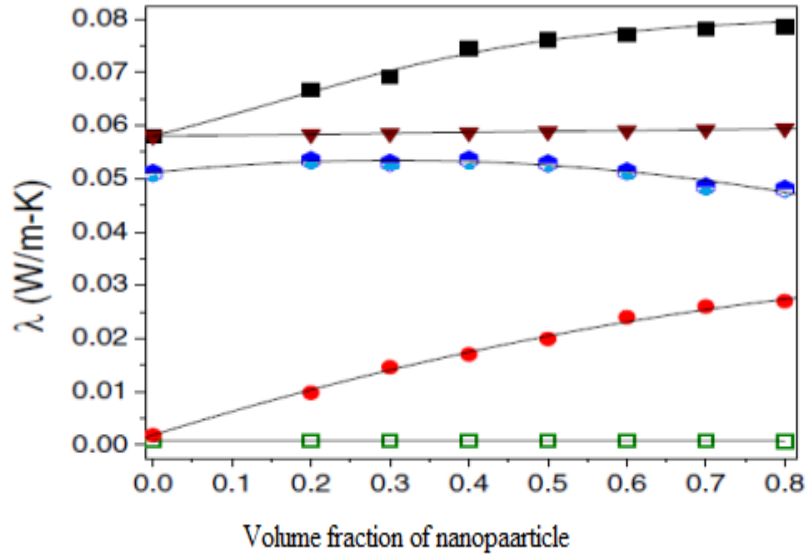


Figure 12: Thermal conductivity of nanocolloid system [58]: λ "■", λ_{kk} "□", λ_{pp} "●", $\lambda_{CC+PC+CP}$ "●" and λ_{MX} "▼".

Since LAMMPS output is discrete, the Green-Kubo formula is used in the software:

$$\lambda = \frac{\Delta t}{3k_B V T^2} \sum_{m=1}^M \frac{1}{N-M} \sum_{n=1}^{N-M} J(m+n)J(n) \quad (4.5)$$

Results and discussions

The thermal conductivity of water was calculated at 300 K and it was used to calculate the thermal conductivity enhancement ratio for copper-water nanofluid. The thermal conductivity predictions of nanofluid were found at nanoparticle volume percent of 2.0%, 2.8%, 5.1%, 6.0% and 9.1%. The predicted values were compared with other obtained values taken from literature. Also, the results showed how the increase in the interatomic interactions among the nanofluid constituents correlates with the increase in the thermal conductivity of the nanofluid.

4.1 Thermal conductivity of water

The thermal conductivity can be found using molecular dynamic simulation by two methods: reverse non-equilibrium molecular dynamic (RNEMD) [38] and equilibrium molecular dynamic (EMD). In contrast to non-equilibrium molecular dynamics (NEMD), the RNEMD imposes a heat flux J_z , in the z -direction for instance (considering an isotropic medium) instead of imposing a temperature gradient, and the temperature gradient is determined instead of the heat flux. Accordingly, the thermal conductivity is expressed as follow

$$k = \lim_{\partial T / \partial z \rightarrow 0} \lim_{t \rightarrow \infty} - \frac{\langle J_z(t) \rangle}{\langle \partial T / \partial z \rangle} \quad (5.1)$$

By using RNEMD [38], the thermal conductivity of water was found to be $\lambda=0.81 \pm 0.01 \text{ W/m} \cdot \text{K}$ at 300 K. On the other hand, the value Bertolini and Tani [35] got for the thermal conductivity of water to be $0.67 \pm 0.04 \text{ W/m} \cdot \text{K}$ at 300 K using EMD simulation; it can be observed that the deviation from the experimental value is 16%.

In this work, the thermal conductivity of pure water has been obtained by performing equilibrium molecular dynamics simulation; then this value was used to get the ratio between thermal conductivity of nanofluid and base fluid ($\frac{\lambda_n}{\lambda_b}$); also the obtained value would reduce the computational errors. The water thermal conductivity has been found to be $\lambda_b = 0.767 \pm 0.01 \text{ W/m} \cdot \text{K}$ at 300 K. It can be observed that the latest obtained value of thermal conductivity of water is more certain than the Bertolini and Tani got but it gives

a percentage difference up to 28 %. In general, EMD method shows to be closer to the experimental value ($\lambda_b = 0.61 \text{ W/m} \cdot \text{K}$) than the mentioned RNEMD method value.

The SPC/E rigid water model had been used to simulate water molecules and perform simulation for different volume fractions of nanofluid. In literature, both SPC/E rigid and flexible are used as models for water. In the recent simulation, the SPC/E rigid was used since it shows a good thermal conductivity value compared to SPC/E flexible value [36, 37].

As it is mentioned before, the initial positions and velocities of molecules should be assigned in order to start the molecular dynamic simulation. In Figure 13, a snapshot was taken from VMD software at initial start of the current water molecular dynamic simulation.

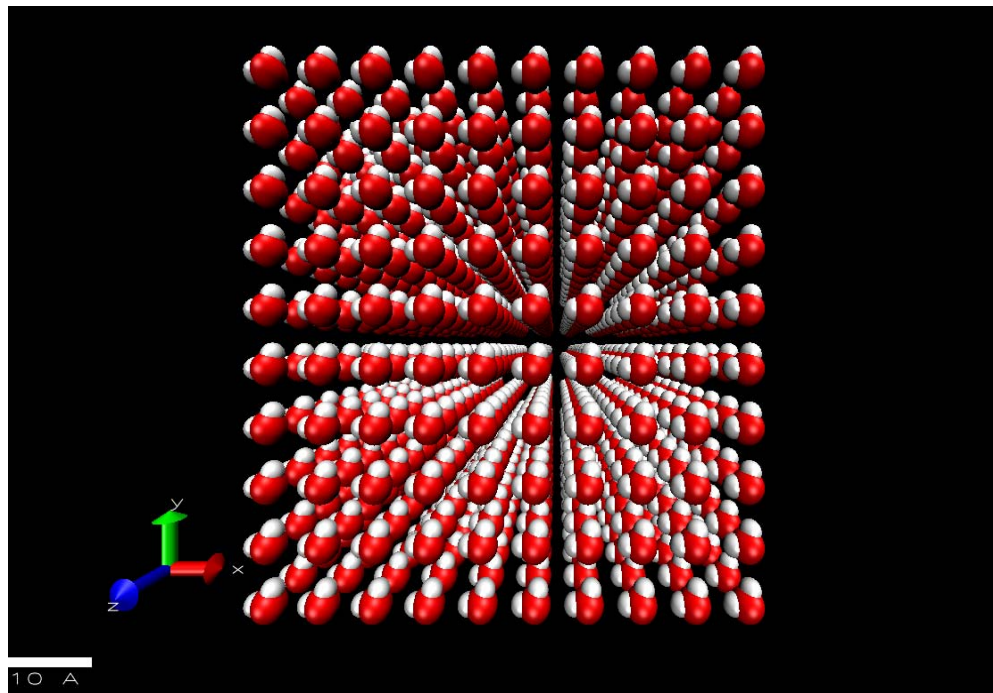


Figure 13: VMD snapshot of initial positions of 991 water monomers.

In order to implement the SPC/E rigid model, the SHAKE algorithm was used with a time step of 0.05 fs and up to 4×10^6 steps. The timestep was chosen carefully in order

to eliminate any round-off or truncation errors; it was performed at 1, 0.05 and 0.025 fs. At 0.05 fs, the result showed to have an accurate and stable value as well as at 0.025 fs.

As it was mentioned in the previous chapter, initial positions and velocities of all water monomers are needed to start the runs of molecular dynamic simulations. Therefore, a MATLAB program was built in order to assign x, y and z coordinates of initial positions for 991 monomers (Figure 13). Initially, the water monomers were confined with an arbitrary simulation box volume of 60850 \AA^3 ($x=39.0 \text{ \AA}$, $y=39.5 \text{ \AA}$ and $z=39.5 \text{ \AA}$); during time evolution of the simulation, the initial volume changed to show the water density, seen in Figure 15. The overlapping of monomers was avoided by placing each monomer 4 \AA away from its neighboring monomers.

Moreover, the initial temperature distribution represents velocity as per equation (3.9). The initial temperature was assigned among the atoms using Gaussian distribution.

During the simulation, the Nosé–Hoover algorithm was used for thermostating at 300 K (see Figure.14).

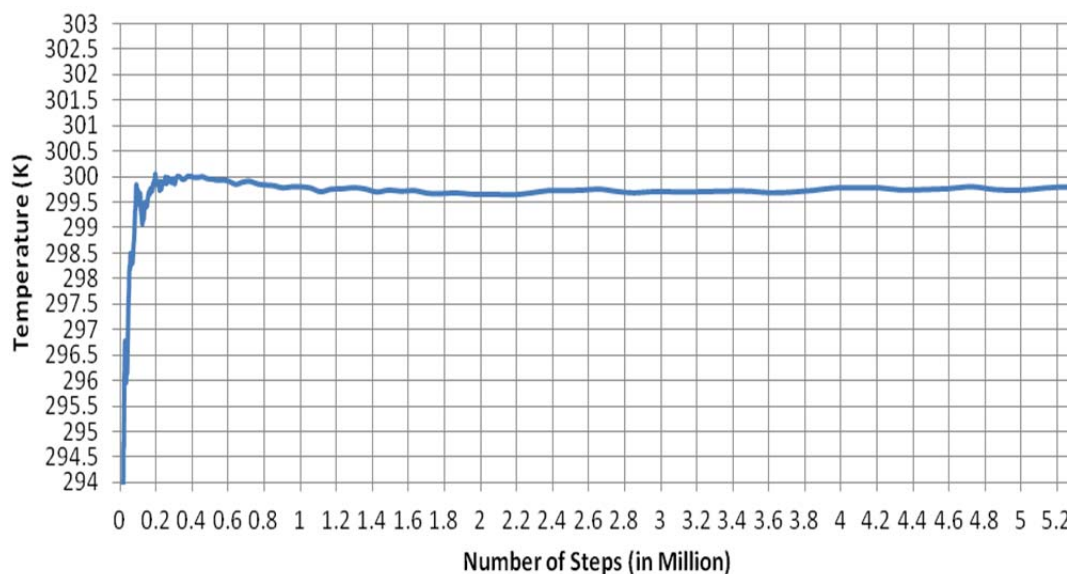


Figure 14: Temperature trend during the simulation.

From the above plot, the temperature appeared after 1×10^6 to be constant at $299.75 \pm 0.25 \text{ K}$ through the molecular simulation and the fluctuations tends to get smaller.

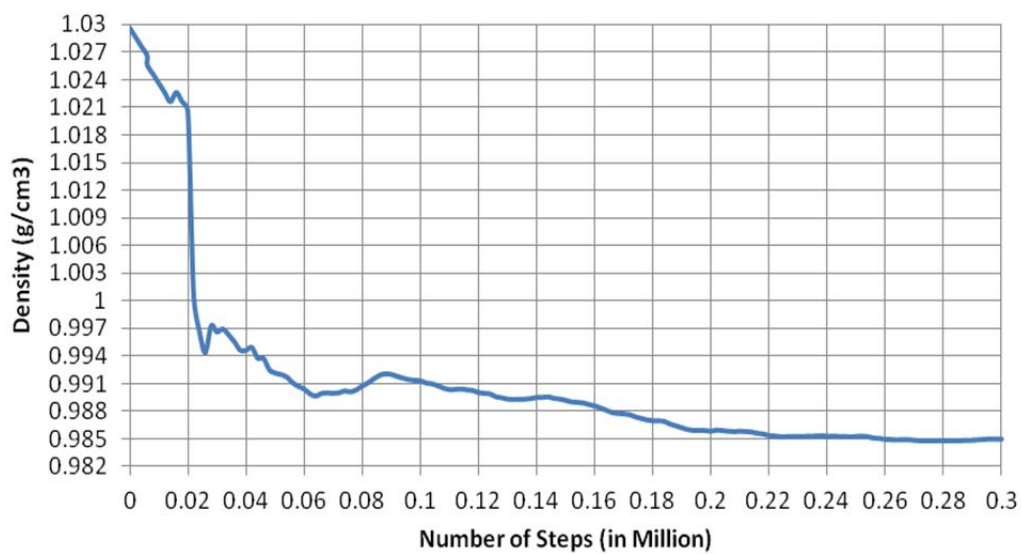


Figure 15: Density of water at 300 K.

Furthermore, the density was obtained at 0.985 g/cm^3 by letting the simulation to run at constant NPT (isothermal-isobaric ensemble) for 2.97×10^5 steps where it showed unchanged density; then the simulation was ran at constant NVT for 6×10^3 steps before starting the sampling. In order to reduce the fluctuations and get accurate results, the samplings were produced for 4×10^6 steps with total running time of 200 ps and the time correlation was taken as 2000 steps (0.1 ps). As per Figure 16, it can be concluded that the heat current autocorrelation function (HCAF) decays to around zero within 700 steps (0.035 ps); therefore, time correlation was adequate for sampling and calculating the thermal conductivity at each time step.

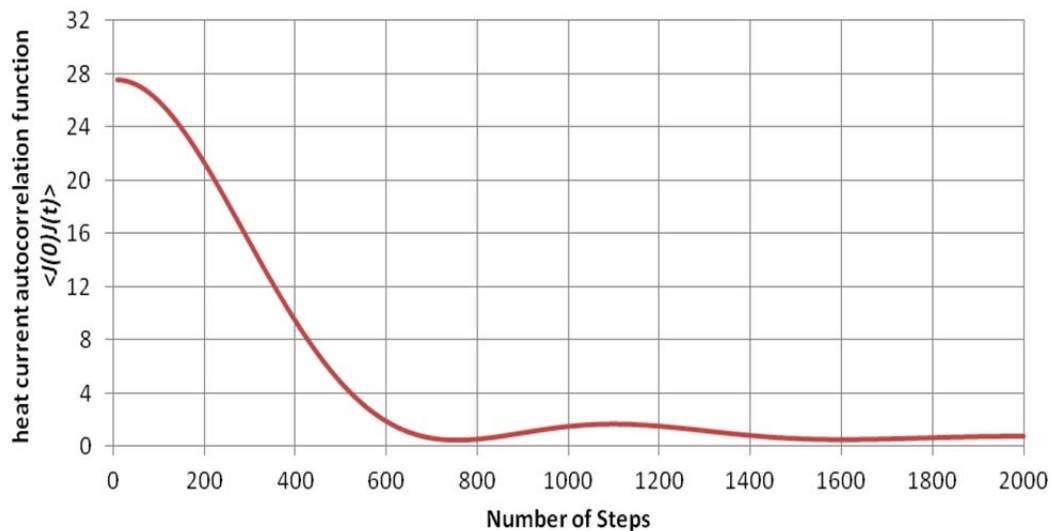
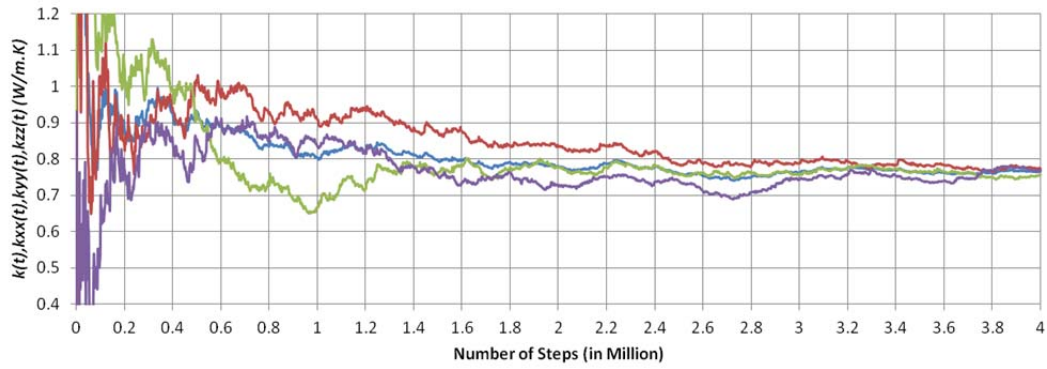


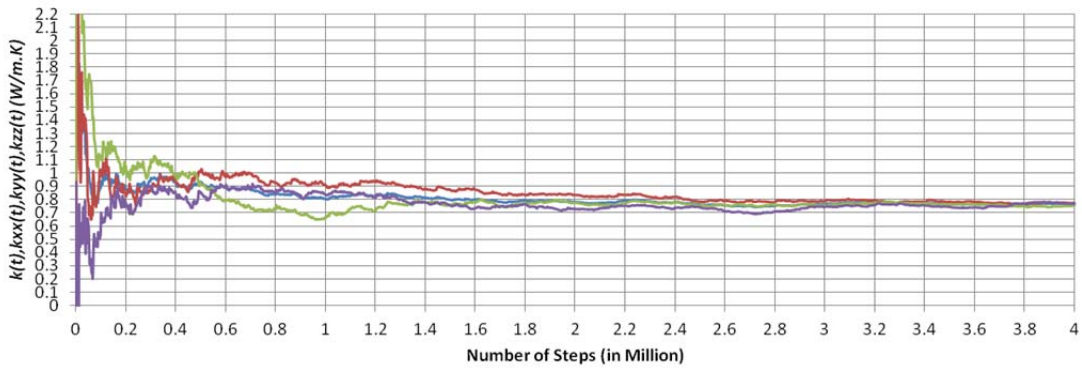
Figure 16: Decay of heat autocorrelation function for water.

The accuracy of the result was determined by comparing the experimental value with the MD value; the certainty of the value was checked by plotting the three vectors of thermal conductivity of water (k_{xx} , k_{yy} and k_{zz}) with their arithmetic averages against time evolution. It showed that the three vectors and their arithmetic average meet at a value that had an acceptable tolerance less than 5% (see Figure 17).

a)



b)



c)

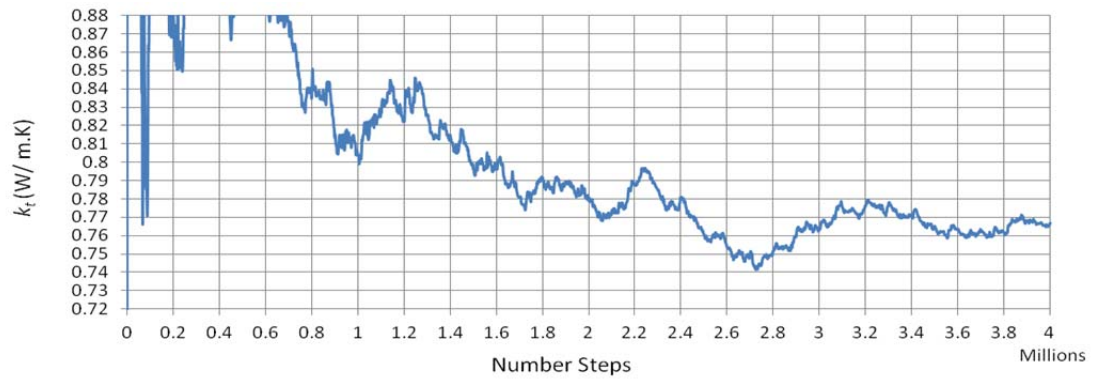


Figure 17: Thermal conductivity of water: a) focused scale, b) full scale, c) overall k . blue line for k , red line for k_{zz} , green line for k_{yy} and purple line for k_{xx} .

Figure 17 shows clearly that the average thermal conductivity of water is $\lambda_b = 0.767 \pm 0.01 \text{ W/m} \cdot \text{K}$ at 300 K and it can be used later in calculating thermal conductivity enhancement ratio of nanofluids.

4.2 Thermal conductivity of nanofluid

From the previous section, modeling and simulating water monomers to find the thermal conductivity was useful in start preparing the nanofluid samples. Nanofluids were modeled and prepared by calculating the required density of nanofluid at different values of volume fraction. The density of nanofluid can be calculated as follows [60]

$$\rho_{nf} = \rho_p \varphi + (1 - \varphi) \rho_{bf} \quad (5.2)$$

Where ρ_p and ρ_{bf} is density of nanoparticles and base fluid, respectively. The density taken for copper nanoparticles is $\rho_p = 8.94 \text{ g/cm}^3$ and for water $\rho_{bf} = 0.985 \text{ g/cm}^3$

Six different samples have been modeled and simulated; one of the samples was shown as in previous section as pure water and other five samples have been modeled by increase the volume percentage of copper nanoparticle to 2.0%, 2.8%, 5.1%, 6.0% and 9.1%. Copper nanoparticle was modeled as a spherical single pseudo atom and inserted to the 991 water monomers (see Figure 18). The initial positions and velocities have no effect on the result after long time evolution.

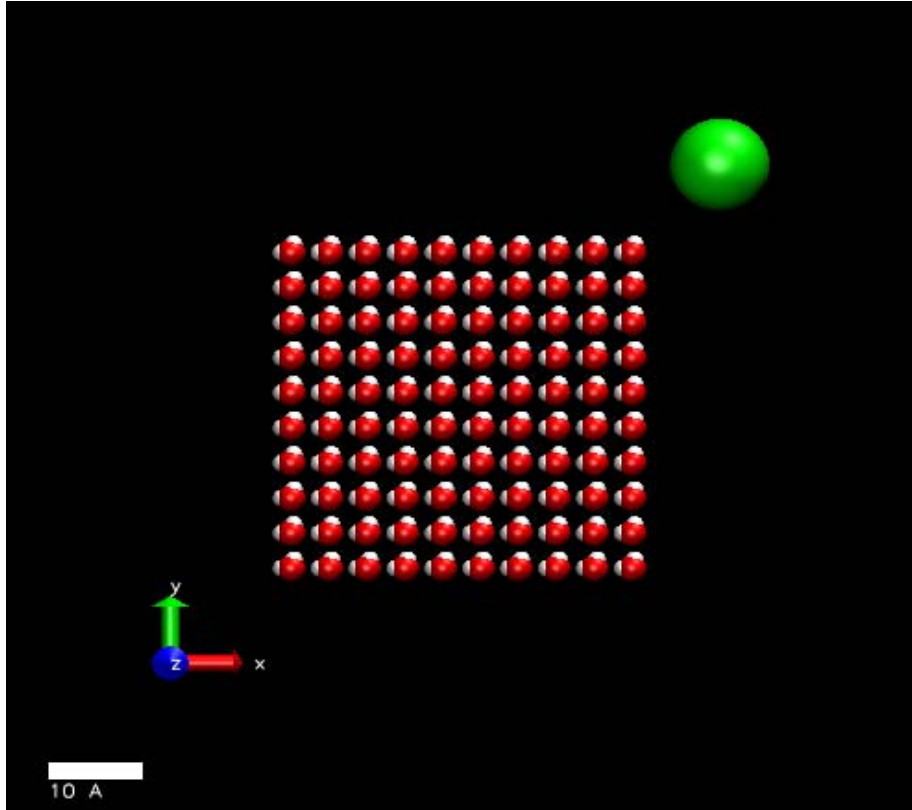


Figure 18: VMD snapshot of initial positions of 991 water monomers and copper nanoparticle.

The radius of the nanoparticles were specified as follows: the first sample as 5.3 Å to meet the volume fraction of 2%, the second sample as 5.9 Å to meet the volume fraction of 2.8%, the third sample as 7.3 Å to meet the volume fraction of 5.2%, the fourth sample as 7.6 Å to meet the volume fraction of 6.0% and the fifth sample as 8.8 Å to meet volume fraction of 9.1%.

The timestep for all samples were chosen to be 0.05 fs as same as water; they were run for many steps till the plot of the three vectors of thermal conductivity of nanofluid (k_{xx} , k_{yy} and k_{zz}) and their arithmetic averages against time evolution shows less fluctuations with acceptable tolerance. Also, the Accuracy was determined by comparing the result of MD with the experimental values in the previous section.

4.2.1. Nanoparticle loading at $\varphi = 2.0\%$

The first sample of nanofluids consists with 2 vol % of copper nanoparticle in water. A single pseudo atom was added as a copper nanoparticle among the 991 water molecules in a confined volume of 30559 \AA^3 . The figure below shows snapshots from VMD during the simulation run; the snapshots are the rotations of the cubical simulation box around y-axis of nanofluid sample at certain time of simulation

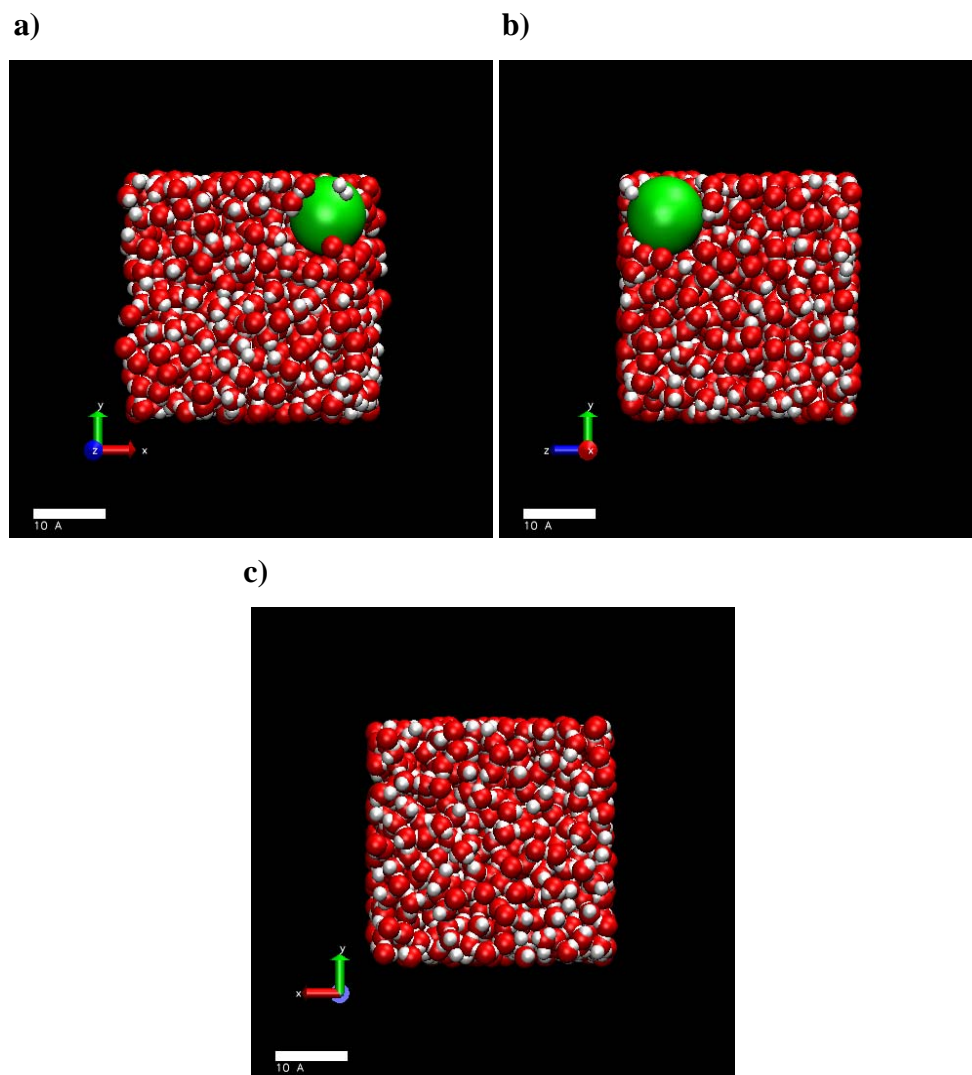


Figure 19: VMD snapshots of 2 vol% nanofluid: **a)** y-x direction (z-axis is out), **b)** y-z direction (x-axis is out), **c)** y-x direction (z-axis is in).

During the simulation, the Nosé–Hoover algorithm was used for thermostating at 300 K while keeping the volume constant (see Figure 20).

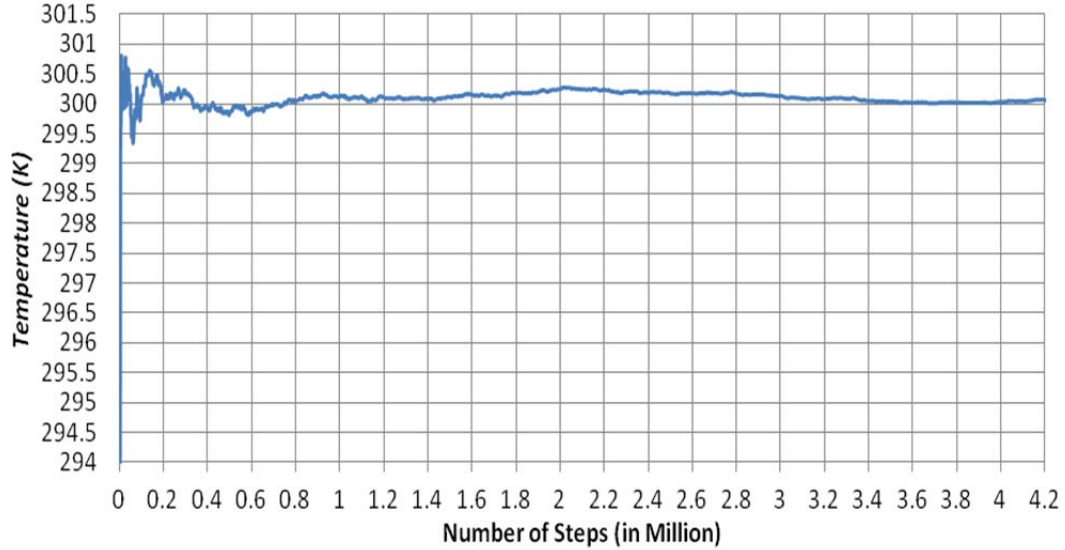


Figure 20: Temperature trend during the simulation.

From the above plot, the temperature appeared after 1×10^6 to be constant at 300 ± 0.01 K through simulation and the fluctuations become small.

Before equilibration, the simulation was run at constant NVT for 3×10^4 in order to set up the temperature of the nanofluid. During the equilibration, the density was held constant at 1.144 g/cm^3 .

The nanofluid density at 2 vol% was calculated using equation (5.3):

$$\begin{aligned} \rho_{nf} &= 8.940 \times 0.02 + (1 - 0.02) \times 0.985 \\ \rho_{nf} &= 1.144 \text{ g/cm}^3 \end{aligned} \quad (5.3)$$

In order to reduce the fluctuations and improve the accuracy in measuring the thermal conductivity of nanofluid, the sampling correlation time and the number of samplings were considered carefully while performing the simulation. The sampling correlation time was taken as 2000 steps (0.1 ps) and the sampling were produced for 3.4×10^6 steps with total running time of 190 ps. As per Figure 21, it can be concluded that the heat current autocorrelation function (HCAF) decays to around zero within 900 steps (0.045 ps);

therefore, time correlation was adequate for sampling and calculating the thermal conductivity at each time step.

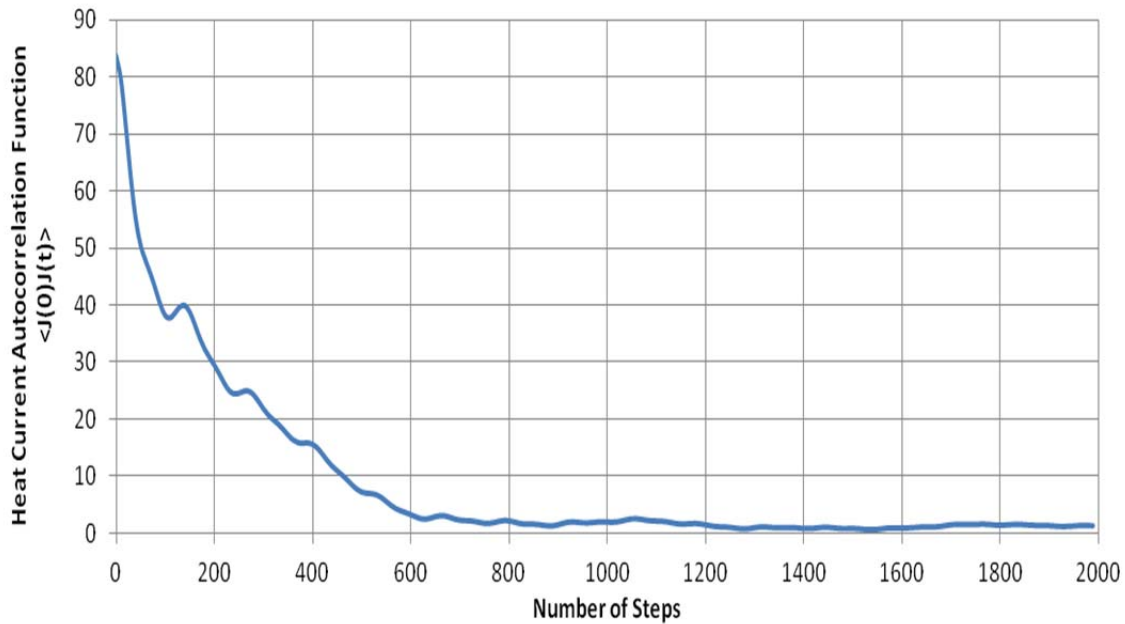
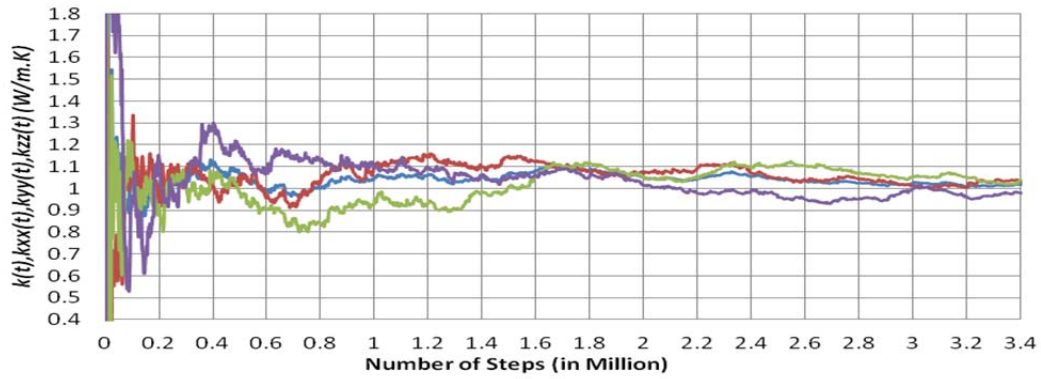


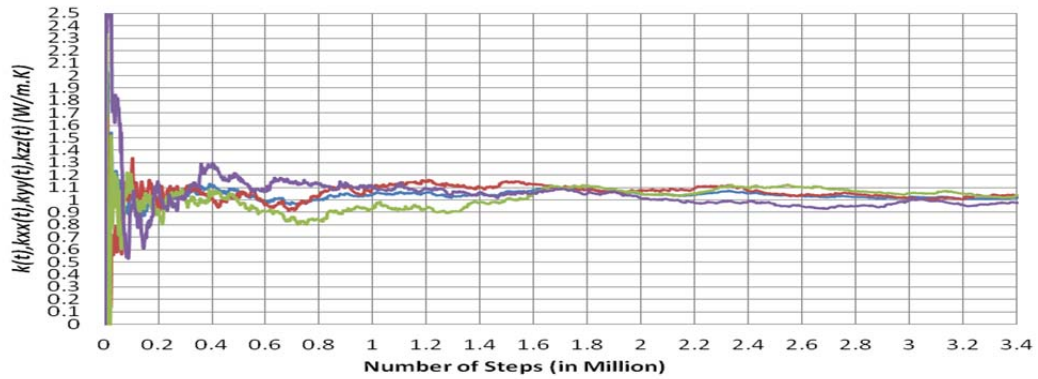
Figure 21: Decay of heat autocorrelation function of nanofluid.

The accuracy of the result was determined by comparing the experimental value with the recent MD value; the certainty of the value was checked by plotting the three vectors of thermal conductivity of nanofluid (k_{xx} , k_{yy} and k_{zz}) with their arithmetic averages against time evolution. It showed that the three vectors and their arithmetic average meet at a value that has an acceptable tolerance less than 5% (see Figure 22).

a)



b)



c)

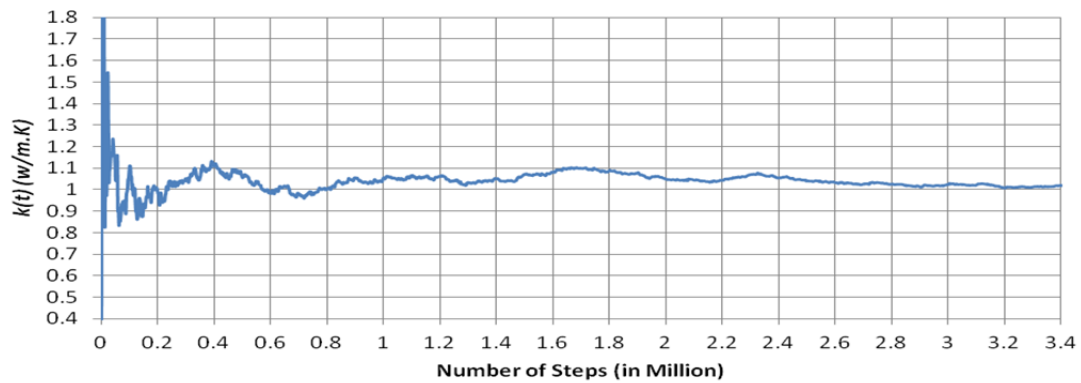


Figure 22: Thermal conductivity of the nanofluid against time evolution $\phi = 2.0\%$: a) focused scale, b) full scale, c) overall k. blue line for k, red line for k_{zz} , green line for k_{yy} and purple line for k_{xx} .

As it is shown in the above Figures, the thermal conductivity was found to be $1.02 \pm 0.02 \text{ W/m} \cdot \text{K}$ at 300 K. Therefore, the thermal conductivity enhancement ratio of 2 vol% nanofluid can be expressed as

$$\frac{\lambda_n}{\lambda_b} = \frac{1.02}{0.767} = 1.33 \quad (5.4)$$

4.2.2. Nanoparticle loading at $\phi = 2.8\%$

The second sample of nanofluids consists of 2.8 vol % of copper nanoparticle in water. A single pseudo atom was added as a copper nanoparticle among the 991 water molecules in a confined volume of 30880 \AA^3 . The figure below shows snapshots from VMD during the simulation run; the snapshots are rotation of the cubical simulation box around y-axis of nanofluid sample at certain time of simulation

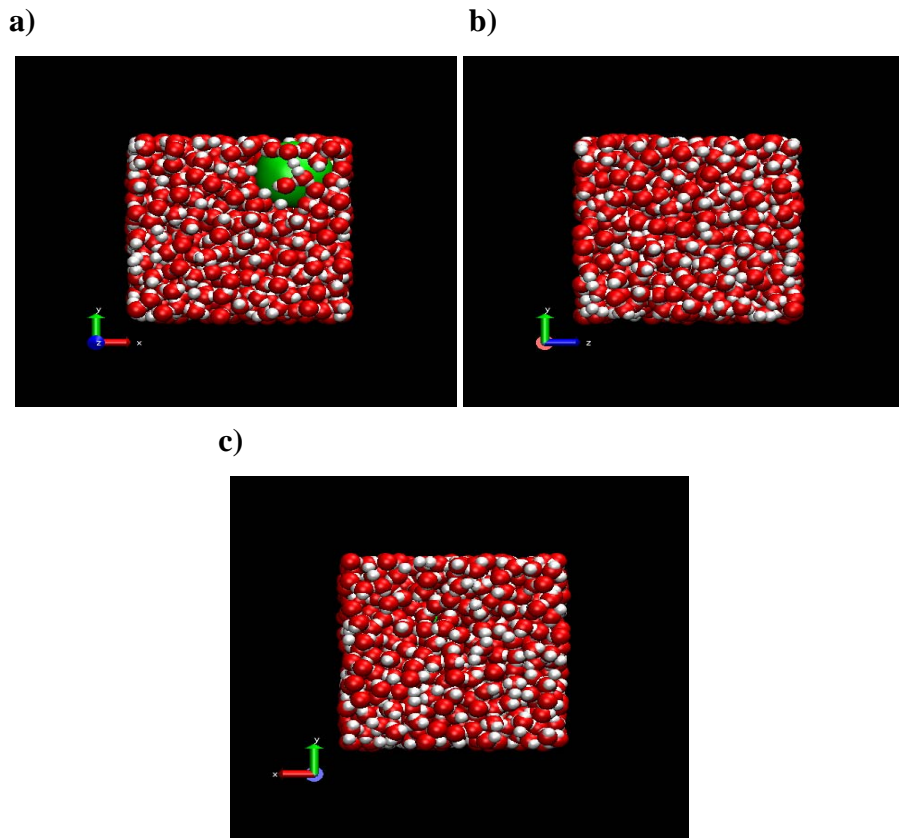


Figure 23: VMD snapshots of 2.8 vol% nanofluid: **a)** y-x direction (z-axis is out), **b)** y-z direction (x-axis is in), **c)** y-x direction (z-axis is in).

The Nosé–Hoover algorithm was used for thermostating at 300 K while keeping the volume constant (see Figure 24).

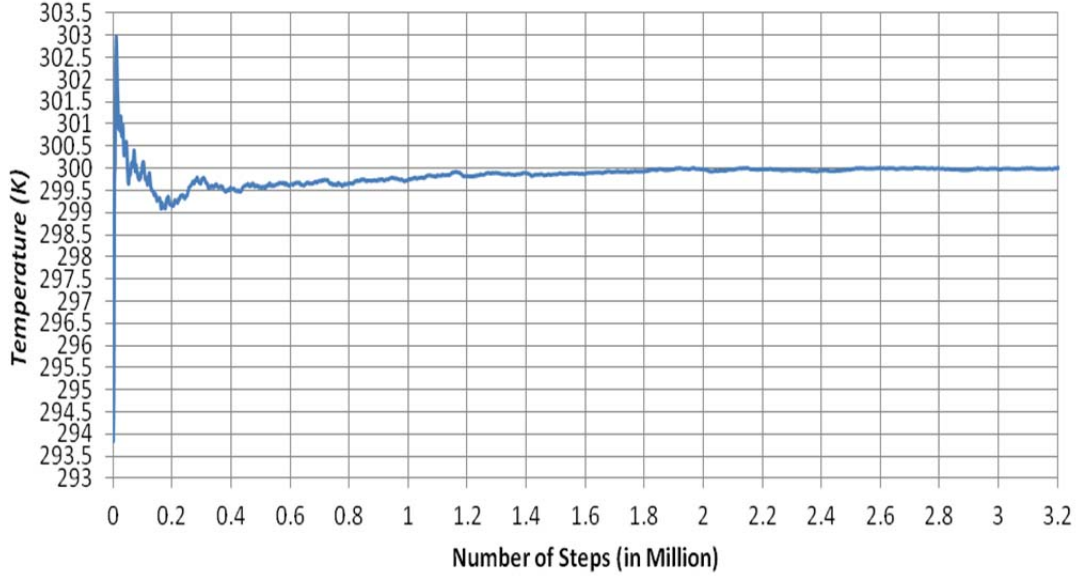


Figure 24: Temperature trend during the simulation.

From the above plot, the temperature appeared after 1.2×10^6 to be constant at 300 ± 0.02 K through the molecular simulation and the fluctuations become small.

Before equilibration, the simulation was run at constant NVT for 3×10^4 in order to set up the temperature of the nanofluid. During the equilibration, the density was held constant at 1.21 g/cm^3 .

The nanofluid density at 2.8 vol% was calculated using equation (5.3):

$$\begin{aligned} \rho_{nf} &= 8.940 \times 0.028 + (1 - 0.028) \times 0.985 \\ \rho_{nf} &= 1.21 \text{ g/cm}^3 \end{aligned} \quad (5.5)$$

In order to reduce the fluctuations and improve the accuracy in measuring the thermal conductivity of nanofluid, the sampling correlation time and the number of samplings were considered carefully while performing the simulation. The sampling correlation time was taken as 2000 steps (0.1 ps) and the samplings were produced for 3.2×10^6 steps with total running time of 190 ps. As per Figure 25, it can be concluded that the heat current autocorrelation function (HCAF) decays to around zero within 900 steps (0.045 ps);

therefore, time correlation was adequate for sampling and calculating the thermal conductivity at each time step.

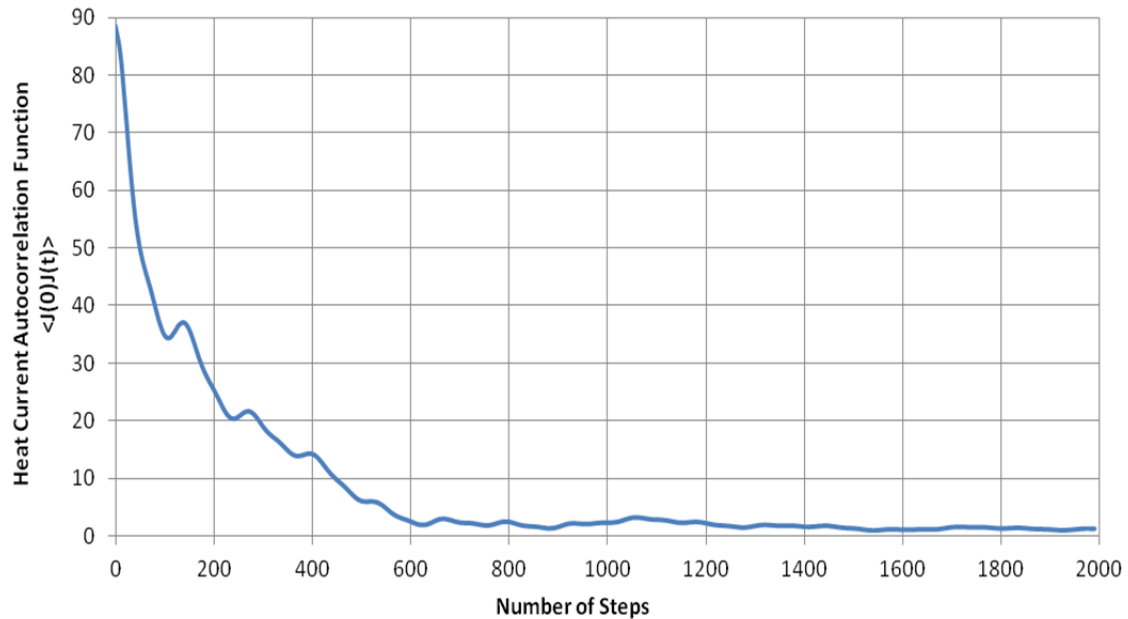
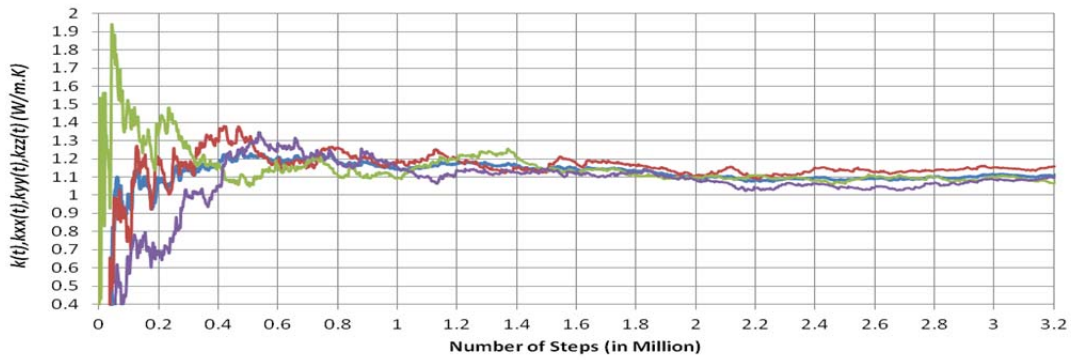


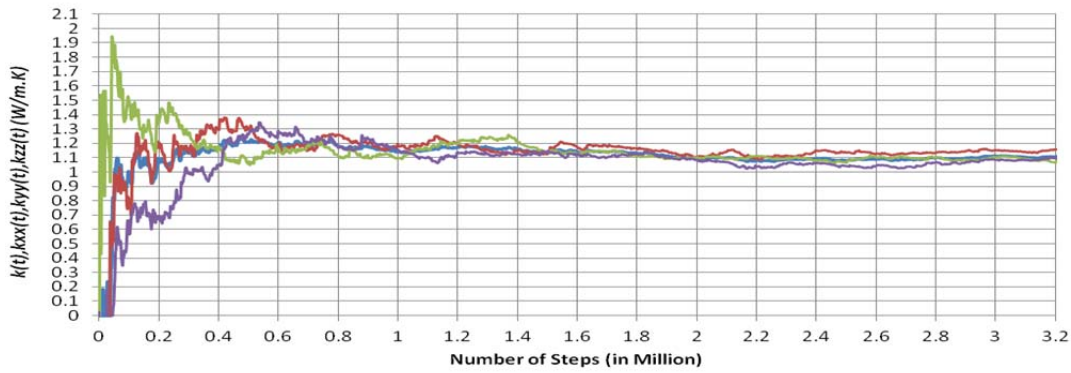
Figure 25: Decay of heat autocorrelation function of nanofluid.

The accuracy of the result was determined by comparing the experimental value with the recent MD value; the certainty of the value was checked by plotting the three vectors of thermal conductivity of nanofluid (k_{xx} , k_{yy} and k_{zz}) with their arithmetic averages against time evolution. It showed that the three vectors and their arithmetic average meet at a value that had an acceptable tolerance less than 5% (see Figure 26).

a)



b)



c)

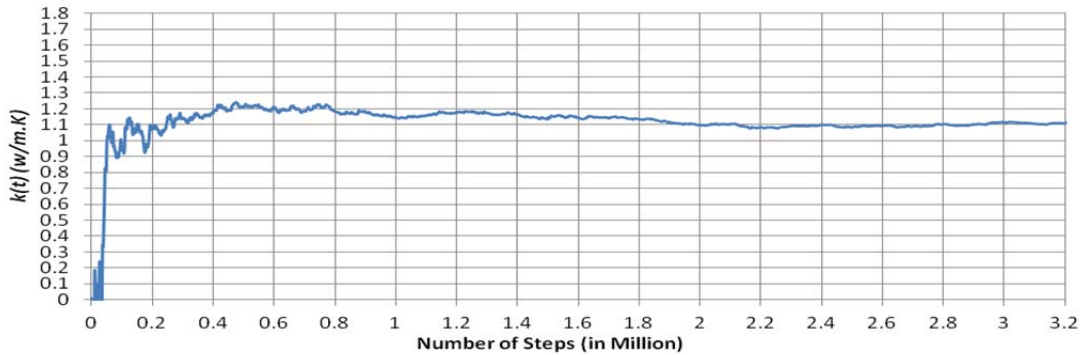


Figure 26: Thermal conductivity of the nanofluid against time evolution $\phi = 2.8\%$: a) focused scale, b) full scale, c) overall k. blue line for k, red line for k_{zz} , green line for k_{yy} and purple line for k_{xx} .

As it is shown in the above Figures, the thermal conductivity was found to be at $1.10 \pm 0.05 \text{ W/m} \cdot \text{K}$. Therefore the thermal conductivity enchantment ratio can be expressed as

$$\frac{\lambda_n}{\lambda_b} = \frac{1.1}{0.767} = 1.43 \quad (5.6)$$

4.2.3. Nanoparticle loading at $\phi = 5.2\%$

The third sample of nanofluids consists with 5.2 vol% of copper nanoparticles in water. A single pseudo atom was added as a copper nanoparticle among the 991 water molecules in a confined volume of 31049 \AA^3 . The figure below shows snapshots from VMD during the simulation run; the snapshots are rotation of the cubical simulation box around y-axis of nanofluid sample at certain time of simulation.

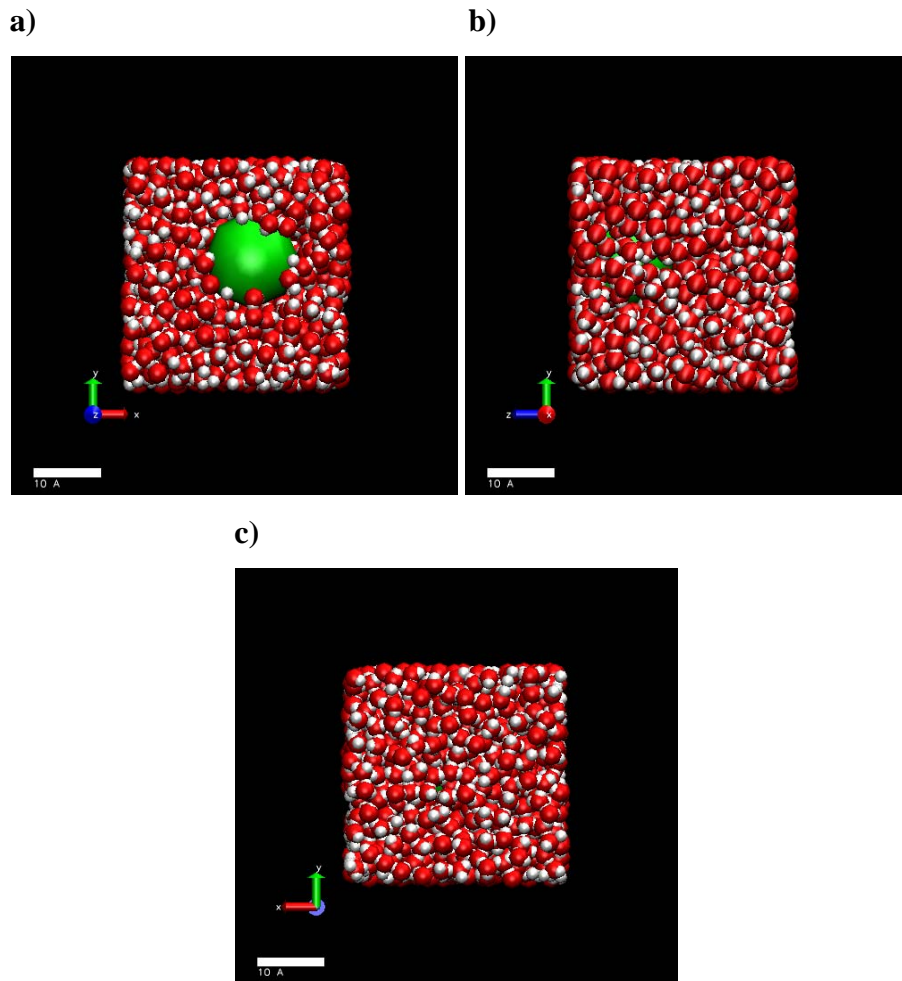


Figure 27: VMD snapshots of 5.2 vol% nanofluid: **a)** y-x direction (z-axis is out), **b)** y-z direction (x-axis is out), **c)** y-x direction (z-axis is in).

The Nosé–Hoover algorithm was used for thermostating at 300 K while keeping the volume constant (see Figure.28).

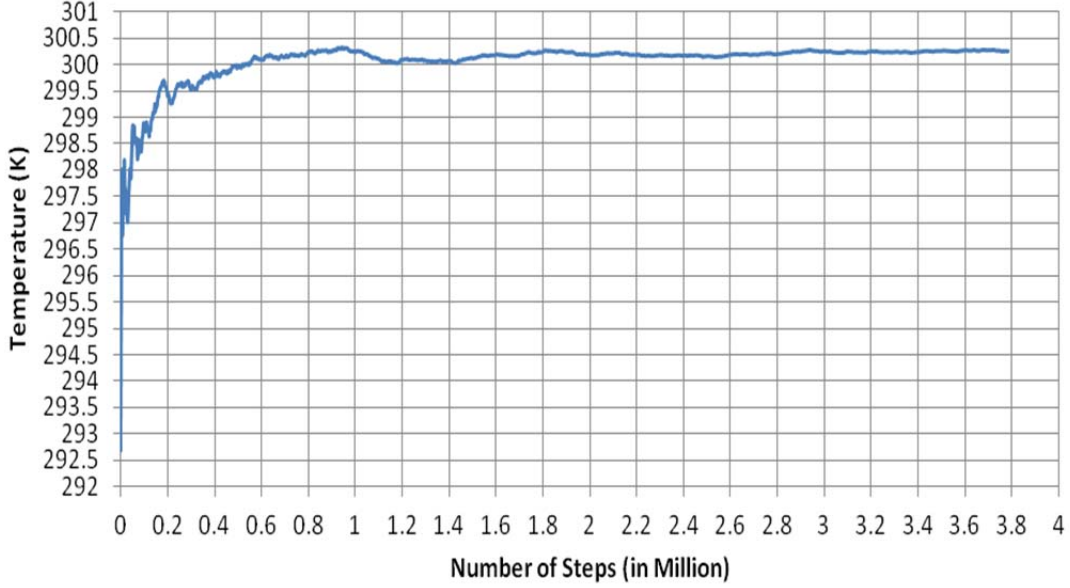


Figure 28: Temperature trend during the simulation.

From the above plot, the temperature appeared after 1×10^6 to be constant at 300 ± 0.02 K through the molecular simulation and the fluctuations become small.

Before equilibration, the simulation was run at constant NVT for 3×10^4 in order to set up the temperature of the nanofluid. During the equilibration, the density was held constant at 1.402 g/cm^3

The nanofluid density at 5.2 vol% was calculated using equation (5.3):

$$\begin{aligned} \rho_{nf} &= 8.940 \times 0.052 + (1 - 0.052) \times 0.985 \\ \rho_{nf} &= 1.402 \text{ g/cm}^3 \end{aligned} \quad (5.7)$$

In order to reduce the fluctuations and improve the accuracy in measuring the thermal conductivity of nanofluid, the sampling correlation time and the number of samplings were considered carefully while performing the simulation. The sampling correlation time was taken as 2000 steps (0.1 ps) and the samplings were produced for 3.8×10^6 steps with total running time of 190 ps. As per Figure 29, it can be concluded that the heat current autocorrelation function (HCAF) decays to around zero within 700 steps (0.035 ps);

therefore, time correlation was adequate for sampling and calculating the thermal conductivity at each time step.

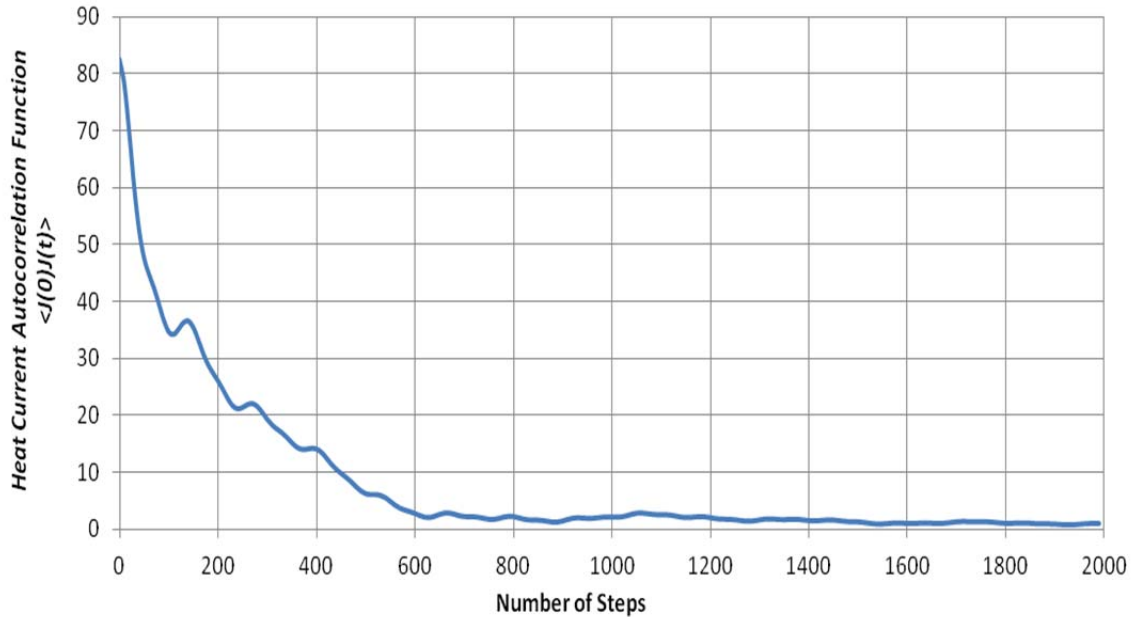
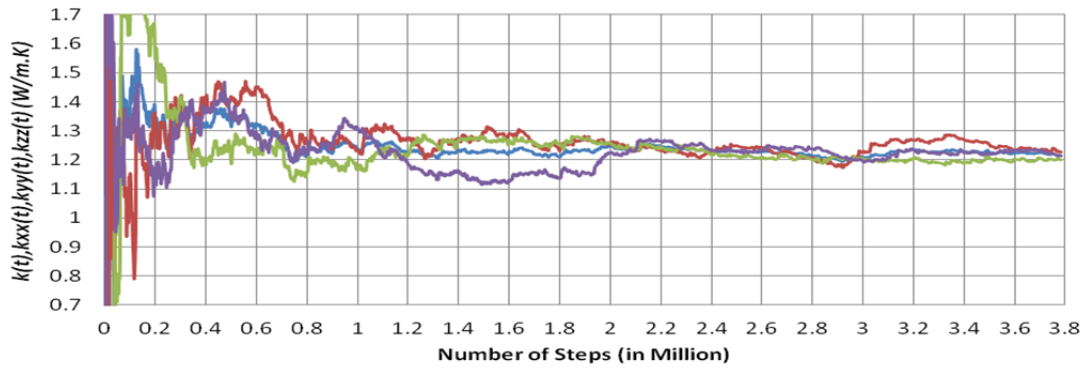


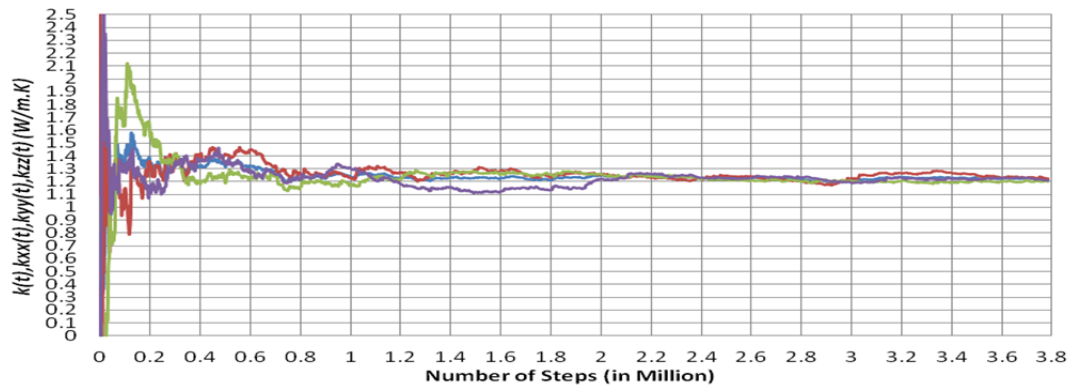
Figure 29: Decay of heat autocorrelation function of nanofluid.

The accuracy of the result was determined by comparing the experimental value with the recent MD value; the certainty of the value was checked by plotting the three vectors of thermal conductivity of nanofluid (k_{xx} , k_{yy} and k_{zz}) with their arithmetic averages against time evolution. It showed that the three vectors and their arithmetic average meet at a value that has an acceptable tolerance less than 5% (see Figure 30).

a)



b)



c)

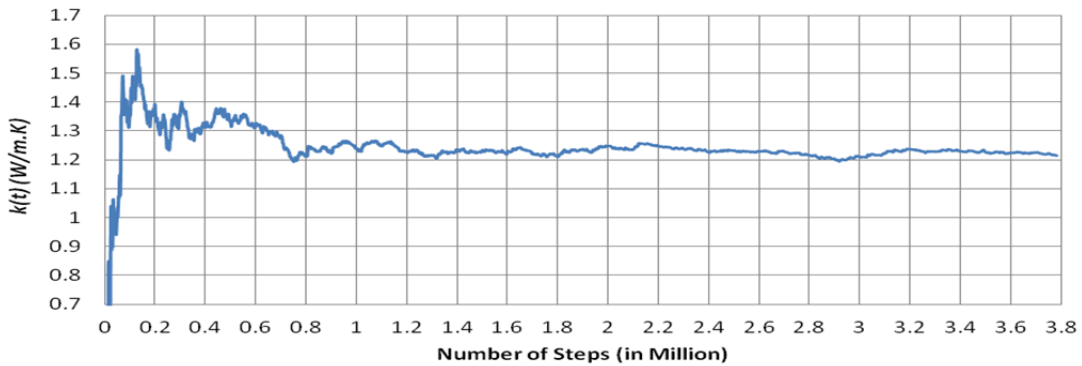


Figure 30: Thermal conductivity of nanofluids against time evolution $\phi = 5.2\%$: a) focused scale, b) full scale, c) overall k. blue line for k, red line for k_{zz} , green line for k_{yy} and purple line for k_{xx} .

As it is shown in the above Figures, the thermal conductivity is found to be at $1.215 \pm 0.015 \text{ W/m} \cdot \text{K}$. Therefore the thermal conductivity enchantment ratio can be expressed as

$$\frac{\lambda_n}{\lambda_b} = \frac{1.215}{0.767} = 1.584 \quad (5.8)$$

4.2.4. Nanoparticle loading at $\phi = 6.0\%$

The fourth sample of nanofluids consists with 6.0 vol % of copper nanoparticle in water. A single pseudo atom was added as a copper nanoparticle among the 991 water molecules in a confined volume of 31138 \AA^3 . The figure below shows snapshots from VMD during the simulation run; the snapshots are rotation of the cubical simulation box around y-axis of nanofluid sample at certain time of simulation

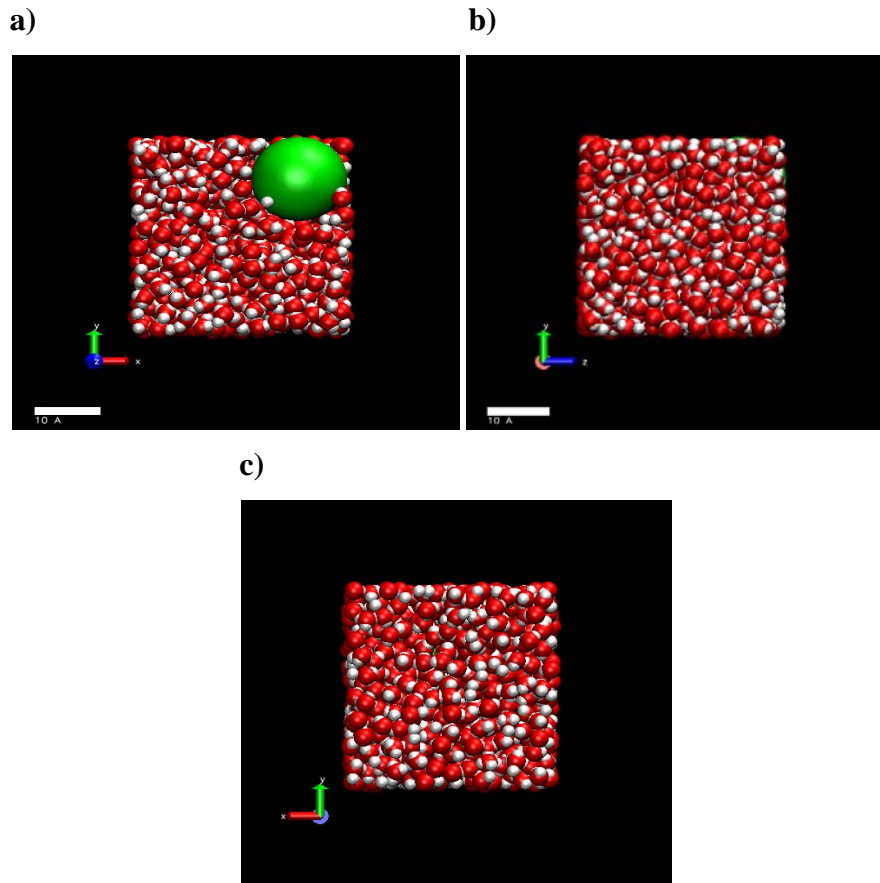


Figure 31: VMD snapshots of 6.0 vol% nanofluid: **a)** y-x direction (z-axis is out), **b)** y-z direction (x-axis is in), **c)** y-x direction (z-axis is in).

The Nosé–Hoover algorithm was used for thermostating at 300 K while keeping the volume constant (see Figure.32).

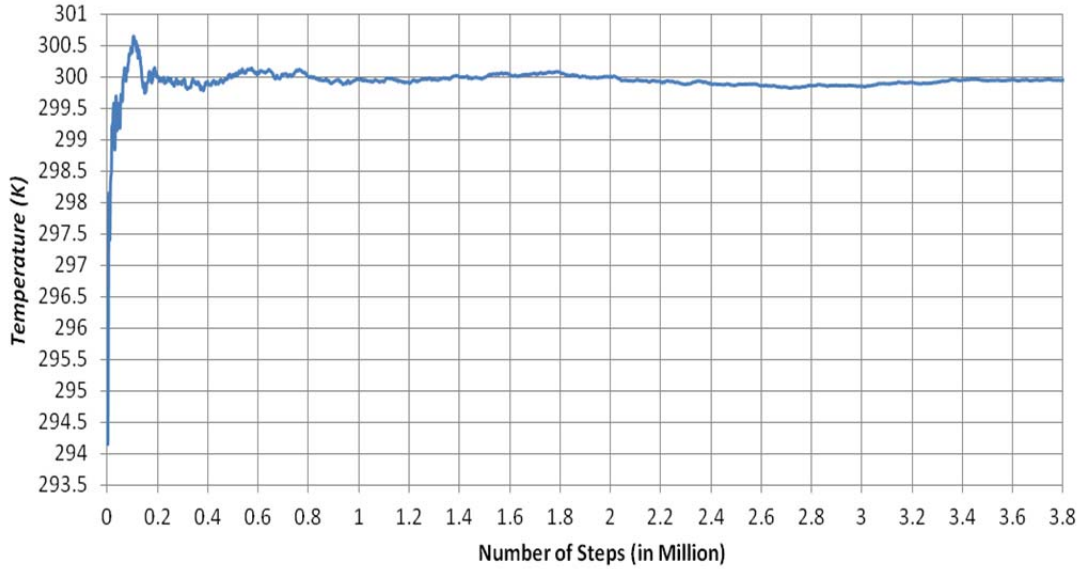


Figure 32: Temperature trend during the simulation.

From the above plot, the temperature appeared after 1×10^6 to be constant at 300 ± 0.01 K through the molecular simulation and the fluctuations become small.

Before equilibration, the simulation was run at constant NVT for 3×10^4 in order to set up the temperature of the nanofluid. During the equilibration, the density was held constant at 1.46 g/cm^3 .

The nanofluid density at 6.0 vol% was calculated using equation (5.3):

$$\begin{aligned} \rho_{nf} &= 8.940 \times 0.06 + (1 - 0.06) \times 0.985 \\ \rho_{nf} &= 1.46 \text{ g/cm}^3 \end{aligned} \quad (5.9)$$

In order to reduce the fluctuations and improve the accuracy in measuring the thermal conductivity of nanofluid, the sampling correlation time and the number of samplings were considered carefully while performing the simulation. The sampling correlation time was taken as 2000 steps (0.1 ps) and the samplings were produced for 3.4×10^6 steps with total running time of 170 ps. As per Figure 33, it can be concluded that the heat current

autocorrelation function (HCAF) decays to around zero within 900 steps (0.045 ps); therefore, time correlation was adequate for sampling and calculating the thermal conductivity at each time step.

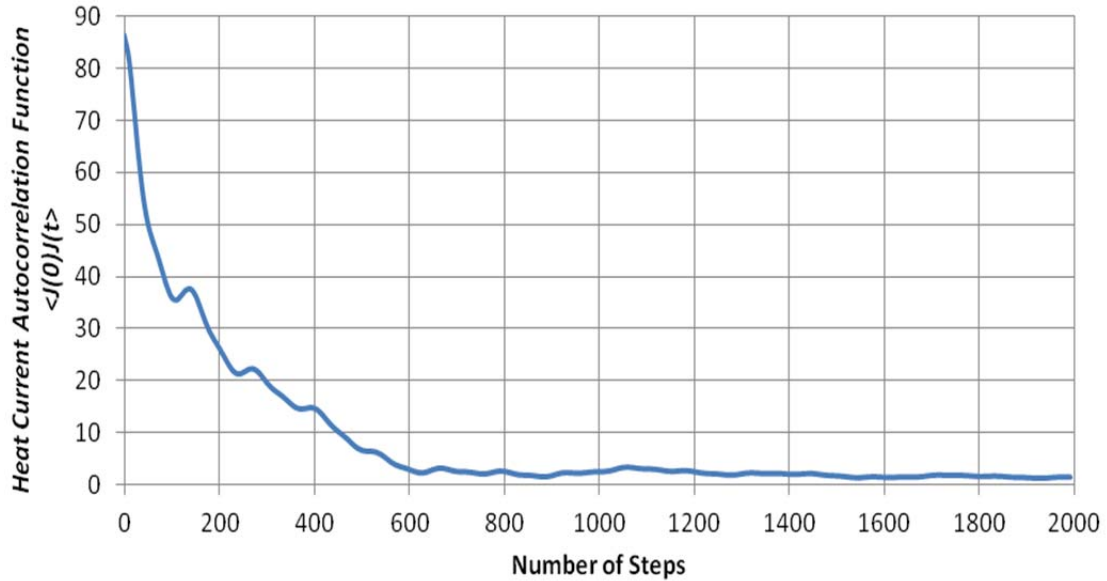
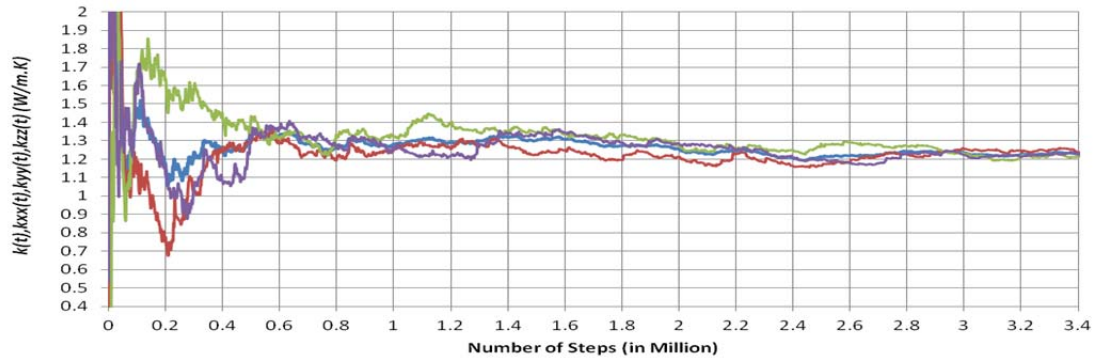


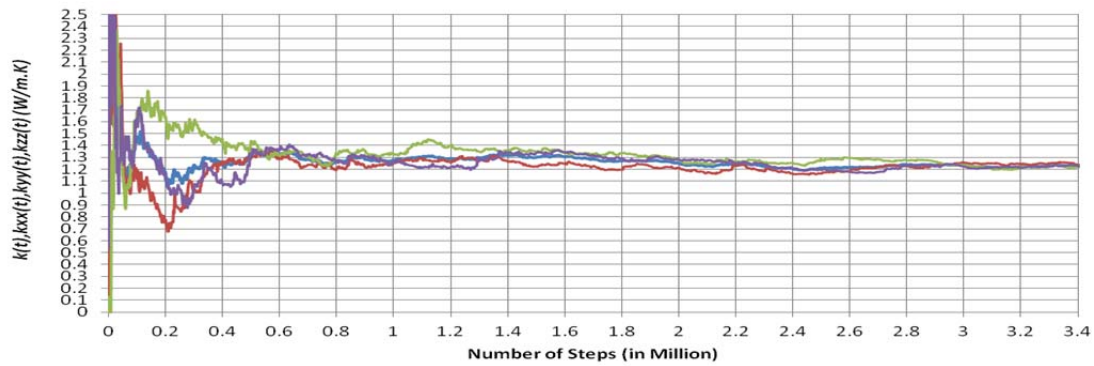
Figure 33: Decay of heat autocorrelation function of nanofluid.

The accuracy of the result was determined by comparing the experimental value with the recent MD value; the certainty of the value was checked by plotting the three vectors of thermal conductivity of nanofluid (k_{xx} , k_{yy} and k_{zz}) with their arithmetic averages against time evolution. It shows that the three vectors and their arithmetic average meet at a value that has an acceptable tolerance less than 5% (see Figure 34).

a)



b)



c)

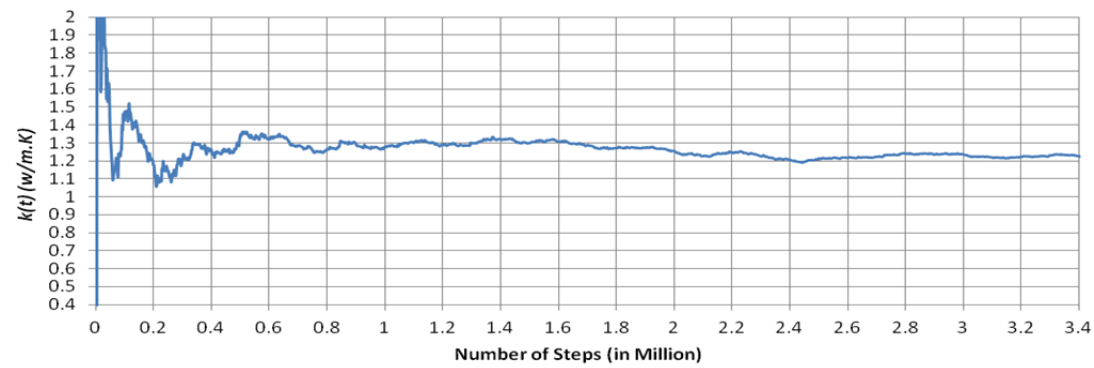


Figure 34: Thermal conductivity of the nanofluid against time evolution $\phi = 6.0\%$: a) focused Scale, b) full scale, c) overall k. blue line for k, red line for k_{zz} , green line for k_{yy} and purple line for k_{xx} .

As it is shown in the above Figures, the thermal conductivity was found to be at $1.24 \pm 0.04 \text{ W/m} \cdot \text{K}$. Therefore the thermal conductivity enhancement ratio can be expressed as

$$\frac{\lambda_n}{\lambda_b} = \frac{1.24}{0.767} = 1.62 \quad (5.10)$$

4.2.5. Nanoparticle loading at $\phi = 9.1\%$

The fifth sample of nanofluids consists with 9.1 vol % of copper nanoparticle in water. A single pseudo atom was added as a copper nanoparticle among the 991 water molecules in a confined volume of 31338 \AA^3 . The figure below shows snapshots from VMD during the simulation run; the snapshots are rotation of the cubical simulation box around y-axis of nanofluid sample at certain time of simulation

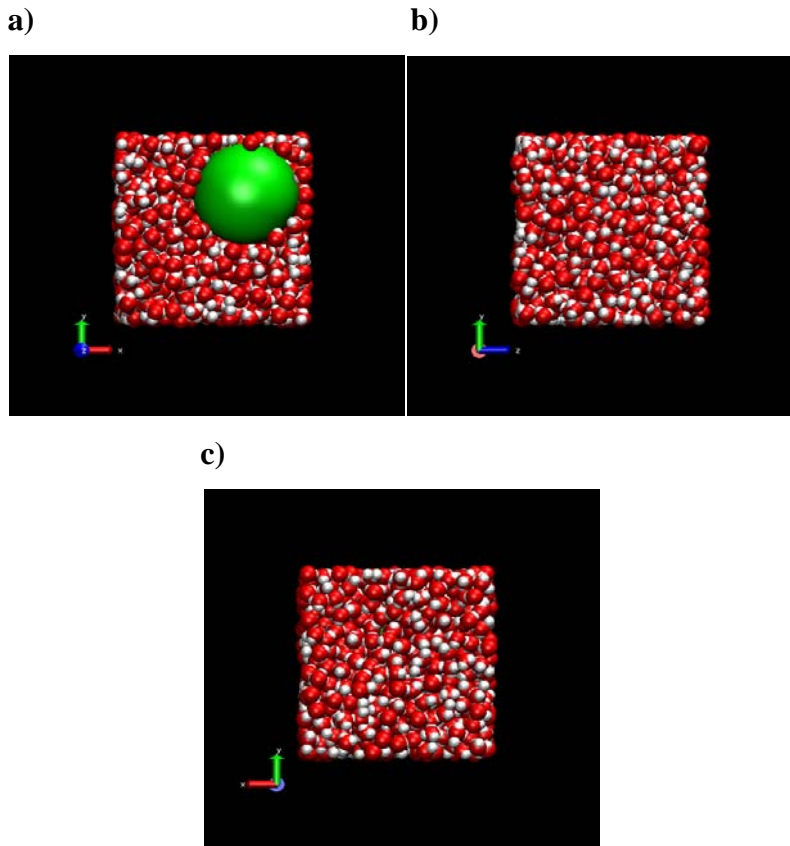


Figure 35: VMD snapshots of 9.1 vol% nanofluid: **a)** y-x direction, **b)** y-z direction, **c)** y-x direction (z-axis is in).

The Nosé–Hoover algorithm was used for thermostating at 300 K while keeping the volume constant (see Figure.36).

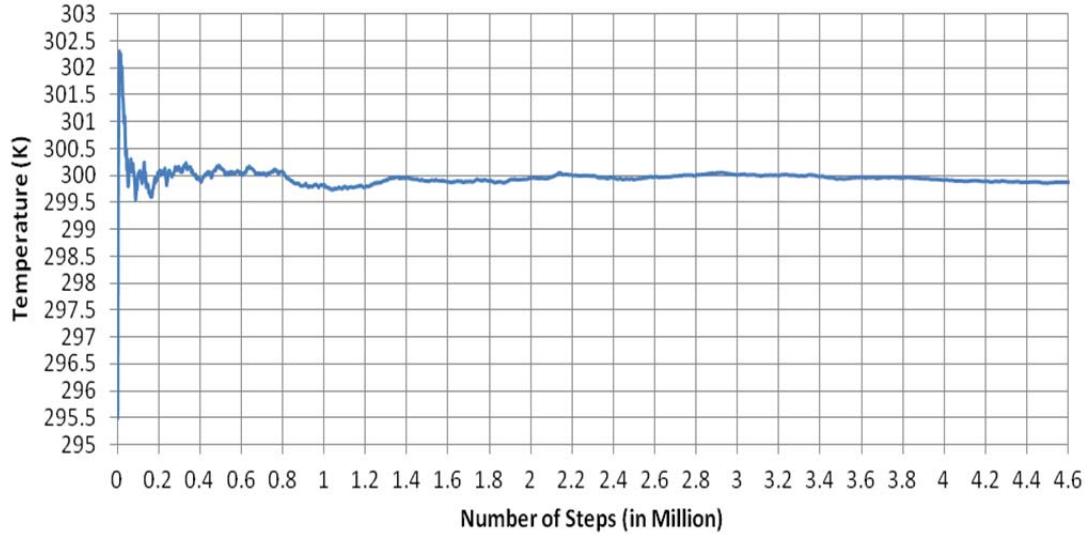


Figure 36: Temperature trend during the simulation.

From the above plot, the temperature appeared after 1×10^6 to be constant at 300 ± 0.01 K through the molecular simulation and the fluctuations become small.

Before equilibration, the simulation was run at constant NVT for 3×10^4 in order to set up the temperature of the nanofluid. During the equilibration, the density was held constant at 1.714 g/cm^3 .

The nanofluid density at 9.1 vol% was calculated using equation (5.3):

$$\begin{aligned} \rho_{nf} &= 8.940 \times 0.091 + (1 - 0.091) \times 0.985 \\ \rho_{nf} &= 1.714 \frac{\text{g}}{\text{cm}^3} \end{aligned} \quad (5.11)$$

In order to reduce the fluctuations and improve the accuracy in measuring the thermal conductivity of nanofluid, the sampling correlation time and the number of samplings were considered carefully while performing the simulation. The sampling correlation time was taken as 2000 steps (0.1 ps) and the samplings were produced for 4.6×10^6 steps with total running time of 230 ps. As per Figure 37, it can be concluded that the heat current autocorrelation function (HCAF) decays to around zero within 1500 steps (0.075 ps);

therefore, time correlation was adequate for sampling and calculating the thermal conductivity at each time step.

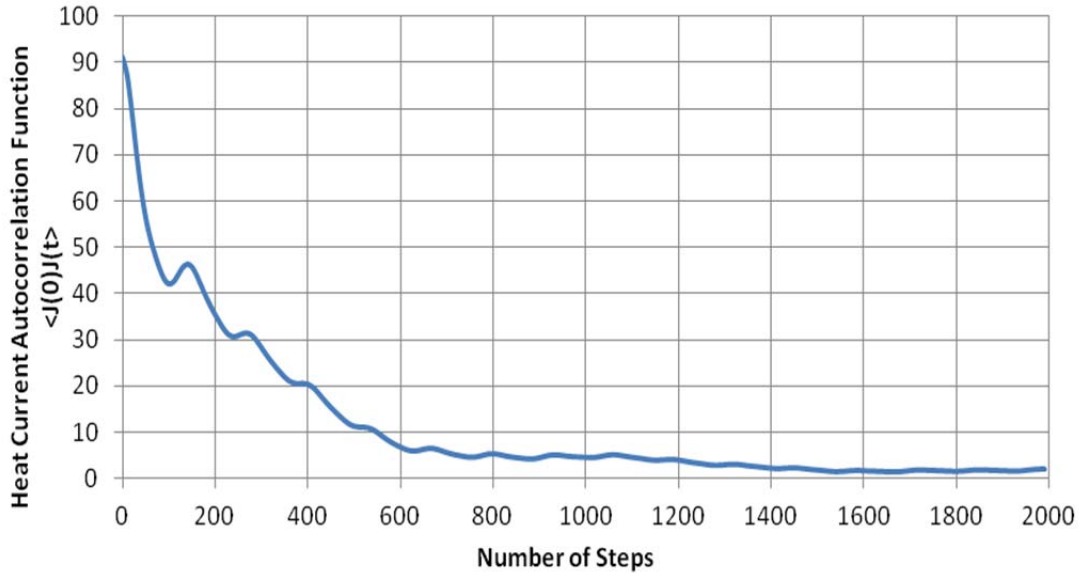
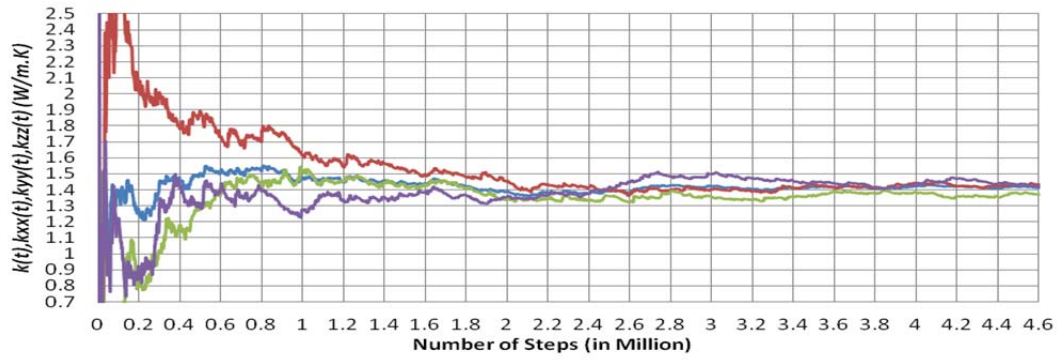


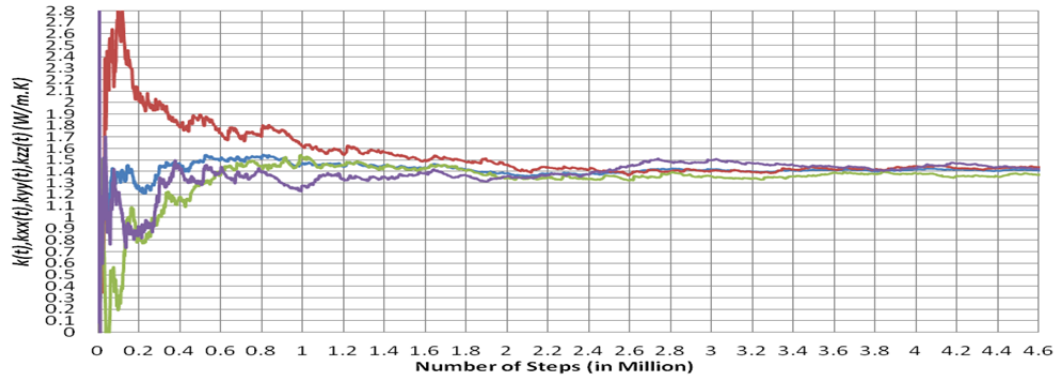
Figure 37: Decay of heat autocorrelation function of nanofluid.

The accuracy of the result was determined by comparing the experimental value with the recent MD value; the certainty of the value was checked by plotting the three vectors of thermal conductivity of nanofluid (k_{xx} , k_{yy} and k_{zz}) with their arithmetic averages against time evolution. It showed that the three vectors and their arithmetic average meet at a value that has an acceptable tolerance less than 5% (see Figure 38).

a)



b)



c)

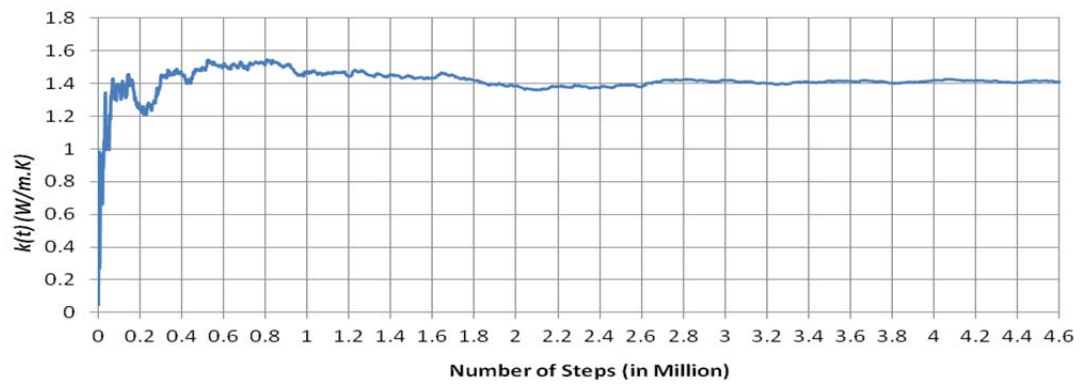


Figure 38: Thermal conductivity of nanofluids against time evolution $\phi = 9.1\%$: a) focused sale, b) full scale, c) overall k. blue line for k, red line for k_{zz} , green line for k_{yy} and purple line for k_{xx} .

As it is shown in the above Figures, the thermal conductivity was found to be at $1.41 \pm 0.031 \text{ W/m} \cdot \text{K}$. Therefore the thermal conductivity enhancement ratio can be expressed as

$$\frac{\lambda_n}{\lambda_b} = \frac{1.41}{0.767} = 1.838 \quad (5.12)$$

4.3 Experimental data with MD results

Xuan and Li experimentally obtained the thermal conductivity of copper and copper-oxide in water and transformer oil. For the copper-water nanofluid, 9% of the laurate salt was added to enhance the stability of nanoparticles suspensions. Xuan and Li discussed the effects of some factors such as the volume fraction, dimensions, shape, and properties of the nanoparticles in improving the heat transfer of the nanofluids. The hot-wire, which is a measurement apparatus, was used by Xuan and Li to measure the thermal conductivity of the nanofluid [5, 61]. Xuan and Li results were consistent with many previous experiments that had shown that increasing the volume fraction of nanoparticles in the base fluid can enhance the thermal conductivity of nanofluids [3, 61, 63].

In this work, the molecular dynamic simulation was performed to show the relation between the thermal conductivity of nanofluids and volume fraction of nanoparticles. In addition, the role of the interatomic interaction in enhancing the thermal conductivity of nanofluid was checked. As seen in Figure 39, the molecular simulation results were compared with the experimental data that Xuan and Li [5, 61] obtained using two different sets of experiments; the first set [5] was obtained for copper nanoparticles volume percentages of 2.5%, 5.2% and 7.5% while the second set [61] was attained for copper nanoparticles volume percentages of 0.3%, 0.5%, 0.8%, 1%, 1.2%, 1.5% and 2%. The Figure also shows an experimental set for Xuan et al [62], and low volume percentages of copper nanoparticles by Zhua et al [63].

The thermal conductivity was found for the present molecular dynamic simulation at five different volume percentages: 2.0 %, 2.8 %, 5.2 %, 6.0 % and 9.1 %.

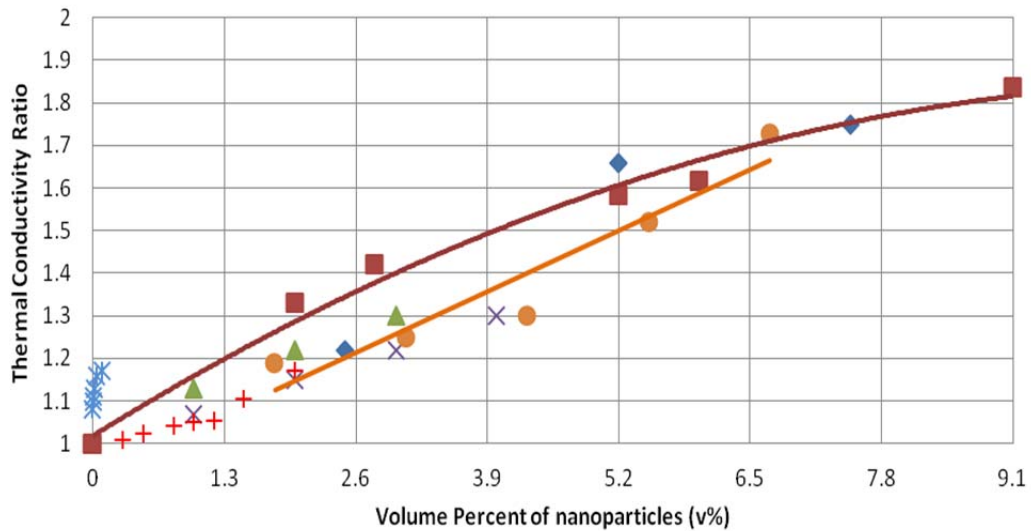


Figure 39: Thermal conductivity enhancement ratio of copper-water nanofluid. The present MD work "■", Xuan et al [61] (r=10nm)"▲", Xuan et al [62] (r=50nm) "×", Xuan and Li (2000) "◆", Xuan and Li (2003) "+", Zhu et al [63] and Sanker et al. MD result"●".

It was observed that the present MD work showed an increasing trend as volume percentages of copper nanoparticles increased; this observation agreed with some other viable experimental data and earlier molecular dynamic simulations. By comparing with different experimental data, it was found that there were differences in values of the enhancement ratios of copper-water nanofluid at very low volume percentages, see above Figure.

Zhu et al. conducted an experiment on copper-water nanofluids to find the thermal conductivity at very low volume percentages between [63] 0.005-0.08%. The nanofluid of volume percentage 0.08 % showed a thermal conductivity enhancement of up to 17% which did not agree with Xuan and Li's results that show 17% enhancement for volume percentage of 2.5%.

From Figure 39, the present MD slightly overestimated Xuan and Li's experimental data for different copper nanoparticle diameters of d=10, 50 and 100 nm; the percentage difference was around 12.5 %. The overestimation especially for low volume percentage

of nanoparticle ($< 4\%$) can be due to the diameter size of the modeled copper nanoparticle; the copper nanoparticle diameters for the present MD were between 5.3 Å to 8.8 Å. On the other hand, the present MD results underestimated the low volume percentage of Zhu's et al. experimental data (up to $\phi = 0.8\%$); the percentage difference was up to 13 %.

The Sanker et al. MD simulation concurred with the present simulation at a higher volume percentage ($>5\%$). In conclusion, thermal conductivity at low volume fraction of nanoparticles is still a topic for further study in order to check for mechanisms or factors that might play an important role in enhancing thermal conductivity using molecular size nanoparticles. The present MD model agreed that very low volume fraction of nanoparticles would significantly enhance the thermal conductivity of nanofluids.

4.4 Role of interatomic potential

In this simulation, the interatomic forces occur mainly due to Van der Waal and Coulombic forces, see section 3.4. The influence of the interatomic forces in enhancing the thermal conductivity of the nanofluid was observed clearly by calculating the Van der Waals and Coulombic potentials. In LAMMPS, the syntax of *evdwl* and *ecoul* were used to calculate the energies of the pure water and the five nanofluid samples that were studied earlier. The kinetic energy was additionally calculated in order to check the Brownian motion of the nanoparticles; *ke* is syntax used for measuring kinetic energy using LAMMPS. As shown in Figure 40, the Kinetic Energy, Van der Waals and Coulombic potentials values of the basic fluid (water) were changed when the copper nanoparticle was added; however, their rates of change as a function of volume percentage of copper nanoparticle were different.

The kinetic energy and Coulombic potential changed as fixed values up to 4% and 49%, respectively. Their values were unvarying in terms of the increase in the volume fraction of the copper nanoparticle. The kinetic energy trend showed and justified that the Brownian motion is very slow and doesn't contribute directly in enhancing the thermal conductivity of nanofluids [2, 21]. The Coulombic potential relates directly to the properties of constituents; since the added nanoparticle was assumed to be neutrally charged, it could be expected that the Coulombic potential would not change as the volume percentage of nanoparticle increased; still, its contribution was remarkable.

Finally, the Van der Waals potential showed to be a function of nanoparticle volume percentage; the change was varying up to 31%.

This study confirmed that the increase in the interatomic interaction, especially Van der Waals and Coulombic interactions enhance the thermal conductivity of nanofluids.

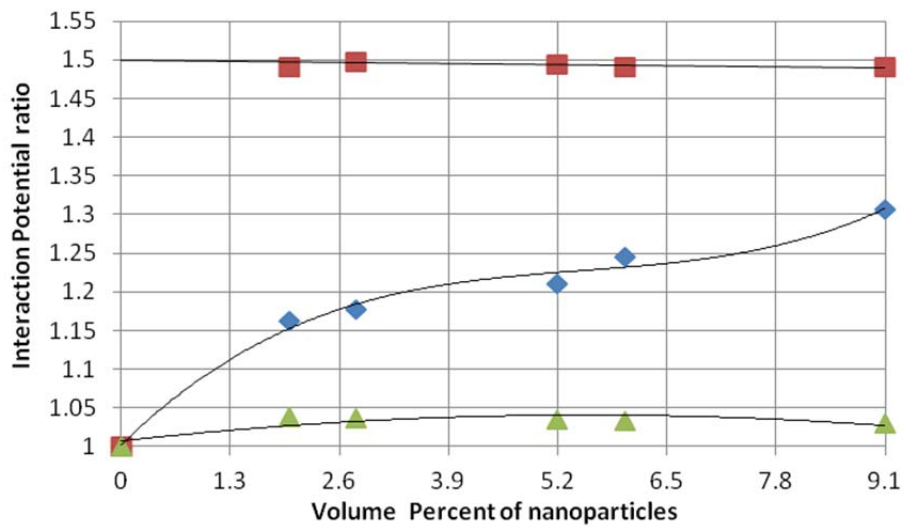


Figure 40: The present MD study showing: kinetic energy "▲", Van- der Waals"◆", Coulombic potentials "■".

Conclusion and recommendations

In this work, the molecular dynamic simulation proved to be one of the practical techniques in predicting transport coefficients of nano-systems. Molecular dynamic simulations have proven to be a good source of finding different thermodynamic and transport properties of nanofluids, such as viscosity, critical heat flux and thermal conductivity. Such properties can be difficult to obtain by experiments or models. In addition, the difficulty in understanding the mechanisms of nano-sized systems through experiments, has given molecular dynamic simulation the chance to be used extensively in modeling and simulating nano-systems for the past 20 years.

In the present work, the obtained thermal conductivity of water reduced the computational errors for calculating the enhancement ratio of the thermal conductivity of nanofluids. The thermal conductivity values of water were found using different molecular dynamic methods like RNEMD and EMD via Green-Kubo; the hydrodynamic generalized method that Bertolini used to find the thermal conductivity of water seemed to be the most accurate technique; it gave a percentage difference of up to 10% with experimental values. The present value showed a percentage difference of 26%; yet it was used since the hydrodynamic generalized method would be difficult to simulate the copper-water nanofluids and since the certainty value was higher. The thermal conductivity of water was found to be $\lambda_b = 0.767 \pm 0.01 \text{ W/m} \cdot \text{K}$ at 300 K.

In addition, Lennard-Jones and Hamaker's formula proved to be appropriate potential models that could be used to mimic the nanofluid particles' interactions. Furthermore, the surface chemistry of nanoparticles should be studied in order to form potential models that can be used in modeling and simulating systems with nano-sized particles. From the available experimental data, it was clear that the increase in the volume fraction of nanoparticles enhances the thermal conductivity of nanofluids. The molecular dynamic simulation results showed an overall agreement with reasonable deviation from available experimental data [5, 61, 62]. The deviation for the low volume percentage (1-4%) could

be due to the small diameter size of the modeled copper nanoparticles, which were relatively close to the size of water monomers.

The available experimental data obtained for the thermal conductivity of copper-water nanofluid showed disagreement [5, 62, 63]. Therefore, experiments for measuring the thermal conductivity of copper-water nanofluid are needed especially at low volume percentages of copper nanoparticle loading.

Furthermore, the present molecular dynamic simulation was able to highlight the role of interatomic potential to enhance the thermal conductivity of nanofluids. Thus, molecular dynamics simulations can be a good tool to understand the mechanisms which illustrate the increases in the thermal conductivity of nanofluids.

During the simulation, it was observed that the Brownian motion of the copper nanoparticles was far too slow to transport heat; consequently, the Brownian motion had a minor effect in enhancing the thermal conductivity of nanofluids. On the other hand, the thermal conductivity of nanofluids increases with the increase in the interatomic interactions. Such interactions depend heavily on the nanofluid's constituent's properties. Therefore, nanoparticles and base fluid types have an important role in determining the enhancement rate of the thermal conductivity of nanofluids. In other words, the type of interaction such as Van der Waals, Coulombs or atomic bonds plays a role in determining the interatomic interactions, which in turn enhance the thermal conductivity of nanofluids.

The present work could be extended to investigate some other enhancement mechanisms such as the role of ordered layering of water monomers around the nanoparticles in increasing the thermal conductivity. Other interaction potentials could be considered and the effect of nanoparticles size and clustering could be studied.

References

1. Sanker, N., Mathew, N., & Sobhan, C. (2008). Molecular dynamics modeling of thermal conductivity enhancement in metal nanoparticle suspensions. *International Communications of heat and mass transfer*, 35, 367-872.
2. Sarker, S., & Selvam, R. (2007). Molecular dynamics simulation of effective thermal conductivity and study of enhanced thermal transport mechanism in nanofluids. *Journal of applied physics*, 102, 074302.
3. Wen, D., Lin, G., Vafaei, S., & Zhang, K. (2009). Review of nanofluids for heat transfer applications. *Particuology*, 7, 141-150.
4. Wang, X., & Mujumdar, A. (2007). Heat transfer characteristic of nanofluids: a review. *International journal of thermal sciences*, 46, 1-19.
5. Xuan, Y. (2000). Heat transfer enhancement of nanofluids. *Journal of heat fluid flow*, 21, 58-64.
6. Allen, M. P., & Tildesley, D. J. (2004). *Computer simulation of liquids*. New-York: Oxford University Press.
7. Lloyd, S. (1996). Universal quantum simulators. *Science*, 273, 1073-1078.
8. "The Birth of Nanotechnology". (2006). Nanogallery.info. Retrieved 26 November 2011. "Faraday made some attempt to explain what was causing the vivid coloration in his gold mixtures, saying that known phenomena seemed to indicate that a mere variation in the size of gold particles gave rise to a variety of resultant colors." <http://www.nanogallery.info/nanogallery/?ipg=126>
9. Maxwell, J. C. (1881). *A treatise on electricity and magnetism*. Oxford: Clarendon Press.
10. Das, S. K., Choi, S. U., Yu, W., & Pradeep, T. (2008). *Nanofluids: science and technology*. New Jersey: John Wiley & Sons.
11. Lide, D. R. (Eds.). (2001). *CRC Handbook of Chemistry and physics* (82nd ed.). Boca Raton: CRC Press.
12. Lide, D. R. (Eds.). (2001). *CRC Handbook of Chemistry and physics* (82nd ed.). Boca Raton : CRC Press.

13. Eastman, J. A., Choi, S. U., Li, S., Yu, W., & Thompson, L. J. (2001). Anomalously increased effective thermal conductivities of ethylene glycol based nanofluids containing copper nanoparticles. *Applied physics letters*, 78, 718-720.
14. Bucak, S. (2011). Importance of defining when applying. *Journal of chemical engineering and process technology*, 2. doi:10.4172/2157-7048.1000e101.
15. Zhu, H., Lin, Y., & Yin, Y. (2004). A novel one-step chemical method for preparation of copper nanofluids. *Journal of colloid interface science*, 277, 100–103.
16. Kim, D., Hwang, Y., Cheong, S., Lee, J., Hong, S., Moon, S., Lee, J., & Kim, S. (2008). Production and characterization of carbon nano colloid via one-step electrochemical method. *Journal of nanoparticle research*, 10, 1121-1128.
17. Wu, S., Zhu, D., Zhang, X., & Huang, J. (2010). Preparation and melting/freezing characteristics of Cu/Paraffin nanofluid as phase-change material (PCM). *Journal of american chemical society*, 24, 1894–1898.
18. Murshed, S. M., Leong, K. C., & Yang, C. (2008). Thermophysical and electrokinetic properties of nanofluids-a critical Review. *Applied thermal engineering*, 28, 2109-2125.
19. Biesso, A., Qian, W., Huang, X., & El-Sayed, M. (2009). Gold nanoparticles surface plasmon field effects on the proton pump process of the bacteriorhodopsin photosynthesis. *Journal of american chemistry society*, 131, 2442–2443.
20. Putra, N., Roetzel, W., & Das, S. K. (2003). Natural convection of nano-fluids. *Heat and mass transfer*, 39, 775–784.
21. Das, S. K., Putra, N., & Roetzel, W. (2003). Pool boiling characteristics of nanofluids. *International journal of heat and mass transfer*, 46, 851-862.
22. Koblinski, P., Phillpot, S. R., Choi, S. U., & Eastman, J. A. (2002). Mechanism of heat flow in suspensions of nano-sized particles. *International journal of heat and mass transfer*, 45, 855-863.
23. Yu, W., & Choi, S. U. (2003). The role of interfacial layers in the enhanced thermal conductivity of nanofluids: a renovated Maxwell model. *Journal of nanoparticle research*, 5, 167-177.
24. Metropolis, N. (1987). The beginning of the Monte Carlo method. *Los Alamos Science*, 15, 125-130.

25. Allen, M. P., & Tildesley, D. J. (2004). *Computer simulation of liquids*. New-York: Oxford University Press.
26. Wood, W., & Jacobson, J. D. (1957). Preliminary results from a recalculation of the Monte Carlo equation of state of hard spheres. *Journal of chemical physics*, 27, 1207-1208.
27. Alder, B. J., & Wainwright, T. E. (1957). Phase transition for a hard sphere system. *Journal chemical physics*, 27, 1208-1209.
28. Rahman, A. (1964). Correlation in the motion of atoms in liquid Argon. *Physical review*, 136, 405–411.
29. Verlet, L. (1967). Computer “experiments” on classical fluid. I thermodynamical properties of Lenard Jones molecules. *Physical review*, 159, 98-103.
30. Kubo, R. (1957). Statistical-mechanical theory of irreversible processes: I. General theory and simple applications to magnetic and conduction problems. *Journal of the physical society of Japan*, 12, 570–586.
31. Hoover, W. G. (1990). *Computational statistical mechanics*. The Livermore National Laboratory.
32. Rapaport, D. C. (2004). *The art of molecular dynamics simulation* (2nd ed.). New-York: Cambridge University Press.
33. Mark, P., & Nilsson, L. (2001). Structure and dynamics of the TIP3P, SPC, and SPC/E water models at 298 K. *Journal of physical chemistry A*, 105, 9954-9960.
34. Guevara-Carrion, G., Vrabec, J., & Hasse, H. (2011). Prediction of self-diffusion coefficient and shear viscosity of water and its binary mixtures with methanol and ethanol by molecular simulation. *The Journal of chemical physics*, 134, 074508.
35. Bertolini, D., & Tani, A. (1997). Thermal conductivity of water: Molecular dynamics and generalized hydrodynamics results. *Physical review E*, 56, 4135-4151.
36. Tironi I., Brunne, R., & Van Gunsteren, W. F. (1996). On the relative merits of flexible versus rigid models for use in computer simulations of molecular liquids. *Chemical physics letters*, 250, 19-24.

37. Habershon, S., Markland, T., & Manolopoulos, D. (2009). Competing quantum effects in the dynamics of a flexible water model. *The journal of chemical physics*, 131, 024501.
38. Zhang, M., Lussette, E., Souza, L., & Muller-Plathe, F. (2005). Thermal conductivities of molecular liquids by reverse non-equilibrium molecular dynamics. *Journal of physical chemistry B*, 109, 15060-15067.
39. Maxwell, J. C. (1891). *A treatise on electrical and magnetism* (3rd ed.). Oxford: Oxford University Press.
40. Jeffrey, D. J. (1973). Conduction through a random suspension of spheres. *Proceedings of royal society of London series A*, 335, 355-367.
41. Davis, R. H. (1986). The effective thermal conductivity of a composite material with spherical inclusions. *International journal of thermophysics*, 7, 609-620.
42. Bruggeman, D. A. (1935). Berechnung verschiedener physikalischer konstanten von heterogenen substanzen, I-ielektrizitatskonstanten undleitfahigkeiten der mischkorper aus isotropen substanzen. *Annalen der Physik, Leipzig*, 24, 636-679.
43. Kleinstreuer, C., & Yu Feng, Y. (2011). Experimental and theoretical studies of nanofluid thermal conductivity enhancement: a review. *Nanoscale research letters*, 6, 229-242.
44. Warriar, P., & Teja, A. (2011). Effect of particle size on the thermal conductivity of nanofluids containing metallic nanoparticles. *Nanoscale research letters*, 66, 247-253.
45. Frenkel, D., & Smit, B. (2002). *Understanding molecular dynamics: From Algorithm to Applications* (2nd ed.). New-York: Academic Press.
46. Hail, J. M. (1992). *Molecular dynamics simulation: Elementary Methods*. New-York: John Wiley & Sons.
47. Jones, J. E. (1924). On the Determination of Molecular Fields. *Proceedings of the Royal Society of London*, 106, 441-461.
48. Luty, B., Davis M., Tironi, I., & Van Gunsteren, G. (1994). A Comparison of particle-particle-particle mesh and Ewald methods for calculating electrostatic interactions in periodic molecular systems. *Molecular Simulation*, 11, 11-20.

49. Everaers, R., & Ejtehadiy, M. R. (2003). Interaction Potential for soft and hard ellipsoids. Max-Planck-Institut fur Polymerforschung, 1-8.
50. Tadros, T. (Eds.). (2010). Colloids in Paints: Colloids and Interface Science. Weinheim: Wiley-VCH.
51. Pashley, R., & Karaman, M. E. (2004). Applied colloid and surface chemistry. West Sussex: John Wiley & Sons Ltd.
52. Bott, T. R. (1995). Fouling of heat exchangers. Amsterdam: ELSEVIER Science.
53. Andersen, H. (1983). Rattle: a “Velocity” version of the shake algorithm for molecular dynamics calculations. Journal of computational physics, 52, 24-34.
54. Theoretical and Computational Biophysics Group. Visual Molecular Dynamic (VMD version 1.9) [Software]. Available from <http://www.ks.uiuc.edu/Development/Download/download.cgi?PackageName=VMD>.
55. Sandia National Laboratories. LAMMPS: Large-scale Atomic/Molecular Massively Parallel Simulator (Version 4th of May.2011) [Software]. Available from <http://lammmps.sandia.gov/>.
56. Hunenberger, P. (2005). Thermostat algorithms for molecular dynamics simulations. Advances in polymer science, 173, 105-149.
57. Thijssen, J. (2007). Computational physics (2nd ed.). New York: Cambridge University Press.
58. Eapen, J., Li, J., & Yip, S. (2007). Mechanism of thermal transport in dilute nanocolloids. Physical review letters, 98, 028302.
59. Jain, S., Patel, H. E., & Das, S. K. (2009). Brownian dynamic simulation for the prediction of effective thermal conductivity of nanofluid. Journal of nanoparticale research, 11, 767-773.
60. Pak B. C., & Cho, Y.I. (1998). Hydrodynamic and heat transfer study of dispersed fluids with submicron metallic oxide particles. Experimental heat transfer, 11, 151–70.
61. Xuan, Y., & Li, Q. (2003). Investigation on Convective Heat transfer and flow features of nanofluids. Journal of heat transfer, 125, 151-155.

62. Xuan, Y., Li, Q., & Hu, W. (2003). Aggregation structure and thermal conductivity of nanofluids. *American institute of chemical engineers*, 49, 1038-1043.
63. Li, X. F., Zhu, D. S., Wang X. J., Wang, N., Gao, J. W., & Li, H. (2008). Thermal conductivity enhancement dependent pH and chemical surfactant for Cu-H₂O nanofluids. *Thermochimica Acta*, 469, 98–103.

